Molecular Therapy
Nucleic Acids
Original Article

lncRNA *DDGC* participates in premature ovarian insufficiency through regulating *RAD51* and *WT1*

Duan Li,[1,2,3,4,5,8] Weiwei Xu,[1,2,3,4,5,8] Xiaoyan Wang,[1,2,3,4,5] Yujie Dang,[1,2,3,4,5] Lan Xu,[1,2,3,4,5] Gang Lu,[6] Wai-Yee Chan,[6] Peter C.K. Leung,[7] Shidou Zhao,[1,2,3,4,5] and Yingying Qin[1,2,3,4,5]

[1]Center for Reproductive Medicine, Cheeloo College of Medicine, Shandong University, Jinan, Shandong 250012, China; [2]Key laboratory of Reproductive Endocrinology of Ministry of Education, Shandong University, Jinan, Shandong 250012, China; [3]Shandong Key Laboratory of Reproductive Medicine, Jinan, Shandong 250012, China; [4]Shandong Provincial Clinical Research Center for Reproductive Health, Jinan, Shandong 250012, China; [5]National Research Center for Assisted Reproductive Technology and Reproductive Genetics, Shandong University, Jinan, Shandong 250012, China; [6]CUHK-SDU Joint Laboratory on Reproductive Genetics, School of Biomedical Sciences, the Chinese University of Hong Kong, Hong Kong, China; [7]Department of Obstetrics and Gynaecology, BC Children's Hospital Research Institute, University of British Columbia, Vancouver, BC V5Z 4H4, Canada

The list of long non-coding RNAs (lncRNAs) that participate in the function of ovarian granulosa cells (GCs) is rapidly expanding, but the mechanisms through which lncRNAs regulate GC function are not yet fully understood. Here, we recognized a minimally expressed lncRNA *RP4-545C24.1* (which we named *DDGC*) in GCs from patients with biochemical premature ovarian insufficiency (bPOI). We further explored the role of lncRNA *DDGC* in GC function and its contribution to the development of bPOI. Mechanistically, silencing *DDGC* downregulated *RAD51* by competitively binding with *miR-589-5p*, and this resulted in significant inhibition of DNA damage repair capacity. In addition, decreased expression of *DDGC* promoted ubiquitin-mediated degradation of Wilms tumor 1 (WT1) protein through interactions with heat shock protein 90 (HSP90), which led to aberrant differentiation of GCs. Moreover, *DDGC* was able to ameliorate the etoposide-induced DNA damage and apoptosis *in vivo*. Taken together, these findings provide new insights into the contribution of lncRNAs in POI pathogenesis.

INTRODUCTION

Substantial advances in high-throughput sequencing technologies have shown that the majority of the human genome is transcribed into long non-coding RNAs (lncRNAs) rather than into proteins.[1,2] LncRNAs are highly heterogeneous RNA molecules with lengths exceeding 200 nt, and they play multiple roles in diverse cellular processes.[3,4] Our growing understanding of the tissue and cell specificity of lncRNAs suggests that lncRNAs might also be involved in the development of pathological disorders such as cancers, immune dysfunction, and cardiovascular disease.[5–7] However, clarifying the regulatory role of lncRNAs in ovarian function has not been studied as intensely.

Premature ovarian insufficiency (POI) is one of the most common reproductive disorders, and is defined as the decline or loss of ovarian function before the age of 40 years, affecting ~1% of women of childbearing age, and it is accompanied by long-term health complications.[8,9] A broad range of etiological factors have been studied, such as genetic, autoimmune, and infectious factors,[10] but these well-known causes are behind fewer than half of all cases, implying that other unknown mechanisms or regulators might contribute to the pathogenesis of POI.

The pathology of POI is a multilayered process that is characterized by unbalanced follicle formation, activation, and exhaustion. Granulosa cells (GCs), as a prominent component of ovarian somatic cells, play an essential role in determining the growth or atresia of follicles,[11–13] and loss-of-function mutations in genes regulating the proliferation or differentiation of GCs, such as *BMP15*,[14] *FSHR*,[15] and *WT1*,[16] have been shown to be causative for POI. Also, recent studies in human GC lines have revealed the association between lncRNAs and polycystic ovary syndrome (PCOS).[17,18] However, the mechanisms through which dysfunctional lncRNAs participate in POI development remain poorly understood.

In the present work, RNA sequencing (RNA-seq) identified the differentially expressed lncRNA *DDGC* in GCs from biochemical (b) POI patients and further revealed its regulatory roles in DNA damage repair processes and differentiation *in vitro* and *in vivo*. Mechanistically, *DDGC* sponged *miR-589-5p* to stabilize *RAD51* mRNA, and *DDGC* also regulated the ubiquitin-mediated degradation of the Wilms tumor 1 (WT1) protein through direct interaction with the heat shock 90 (HSP90) protein. Our study suggests that lncRNA *DDGC* is involved in DNA damage repair and in the timely

Received 10 March 2021; accepted 6 October 2021;
https://doi.org/10.1016/j.omtn.2021.10.015.

[8]These authors contributed equally

Correspondence: Yingying Qin, PhD, Center for Reproductive Medicine, Cheeloo College of Medicine, Shandong University, Jinan, Shandong 250012, China.
E-mail: qinyingying1006@163.com

Table 1. Baseline characteristics of study participants for RNA-seq

Characteristic	Control (n = 9)	bPOI (n = 8)	p
Age (years)	32.00 ± 4.15	34.00 ± 4.41	0.351
BMI (kg/m^2)	21.36 ± 1.89	22.33 ± 2.08	0.329
bFSH (IU/L)	6.37 ± 0.85	15.90 ± 3.73	<0.0001
bLH (IU/L)	4.67 ± 2.02	7.55 ± 2.95	0.032
bE2 (pg/mL)	33.89 ± 17.77	28.93 ± 11.93	0.516
AMH (ng/mL)	4.09 ± 2.08	0.63 ± 0.17	<0.001

bFSH, basal FSH; bLH, basal luteinizing hormone; bE2, basal estradiol.
Data are presented as mean ± SD, Students' t test.

differentiation of GCs and thus provides a new epigenetic perspective on POI pathogenesis.

RESULTS

LncRNA *DDGC* is significantly minimally expressed in GCs from bPOI patients

A total of 78 lncRNAs were differentially expressed in GCs between the eight patients and the nine controls (Table 1, Figures 1A and 1B) according to RNA-seq analyses (GSE158526).[19] To validate the RNA-seq results, six lncRNAs with high conservative properties as shown by the UCSC resources[20] were chosen for further detection by qRT-PCR. As shown in Figures 1C and S1, three lncRNAs—*RP4-545C24.1*, *AC112721.1*, and *ZNF674-AS1*—were minimally expressed, and three lncRNAs—*RP11-3D4.3*, *SNAI3-AS1*, and *GS1-358P8.4*—were upregulated in GCs from bPOI patients (Table 2). Among them, lncRNA *RP4-545C24.1*, located at 7q35 and with limited known functions, showed the greatest fold change (Table S1, fold change = 2.12). We assessed the coding potential of *RP4-545C24.1* using the Coding-Potential Calculator[21] and Coding-Potential Assessment Tool,[22] which confirmed the non-coding characteristic of *RP4-545C24.1* (Figure S2A). Furthermore, *RP4-545C24.1* had a relatively high expression level in the ovary according to the Genotype-Tissue Expression database[23] (Figure S2B), which was similar to its expression profile in 21-week human fetal tissues (Figure 1D), suggesting a potential regulatory role in ovarian function. In addition, the single-cell RNA-seq analysis[24] showed that the expression of *DDGC* in human GCs was increased with follicle development (Figure S2C). Therefore, we focused on *RP4-545C24.1* for subsequent experiments. For simplicity, we refer to *RP4-545C24.1* as *DDGC* (DNA damage repair and differentiation of GC regulatory RNA), given its roles in DNA damage repair and differentiation in GCs.

Silencing *DDGC* impairs DNA damage repair by downregulating *RAD51*

Because *DDGC* is a transcript with limited known functions, we analyzed transcriptome data by RNA-seq (GSE158555) in KGN cells upon downregulation of *DDGC* with small interfering RNA (siRNA) (Figure S3A). As shown in Figures 2A and S3B, a total of 728 genes were differentially expressed as a consequence of *DDGC* silencing. Analysis of Kyoto Encyclopedia of Genes and Genomes pathways found that the most significantly enriched pathways included cell-cycle-related pathways, the Fanconi anemia pathway, and the homologous recombination (HR) pathway (Figure 2B), which were confirmed by qRT-PCR analysis (Figures S3C and S3D). Loss-of-function experiments were performed to determine the effect of *DDGC* knockdown in GCs.

As shown in Figures S3E–S3I, CCK8, 5-ethynyl-2′-deoxyuridine (EdU) staining, and flow cytometry analysis showed no significant impact of *DDGC* silencing on cell-cycle progression or proliferation of GCs. To measure DNA damage repair capacity and to evaluate the cellular response to DNA damage induced by etoposide (ETO), γH2AX levels were measured by western blot and immunofluorescence as an indicator of double-strand breaks (DSBs). After exposure to ETO, γH2AX foci were observed and disappeared as the repair process progressed (Figure 2C). *DDGC* silencing significantly prolonged the time to repair ETO-induced DSBs in both KGN and SVOG cells (Figure 2D), which suggested that *DDGC* silencing inhibits the progress of DSB repair in GCs. As a consequence, silencing of *DDGC* significantly increased GC apoptosis as evidenced by increased levels of cleaved poly ADP-ribose polymerase protein (PARP) (Figure 2E) and terminal deoxynucleotidyl transferase dUTP nick-end labeling (TUNEL) signal (Figure 2F). Collectively, these findings suggest that downregulation of *DDGC* inhibits DNA damage repair in GCs.

To clarify the molecular mechanism underlying this phenomenon, we measured the DNA repair proteins that were differentially expressed after *DDGC* knockdown. As shown in Figure 2G, silencing *DDGC* led to a significantly decreased RAD51 protein level, but there was no significant effect on BRCA2, BARD1, or BRCA1 protein levels. Therefore, we next explored whether downregulated *RAD51* was responsible for the impaired DNA damage repair seen in *DDGC*-silenced cells. Downregulation of *RAD51* by siRNA (Figure S3J) impaired DNA damage repair of KGN and SVOG cells (Figure 2H), which mimicked the phenotype upon *DDGC* silencing. Moreover, overexpression of *RAD51* attenuated the levels of γH2AX induced by ETO after *DDGC* silencing (Figures S3K and S3L). Considering the vital role of *RAD51* in the HR repair pathway, we validated the impact of *DDGC* silencing on the repair of DNA damage induced by camptothecin, which can be repaired only through the HR pathway, and not the non-homologous end-joining pathway. Consistent with the results of ETO treatment, γH2AX was observed after camptothecin-induced damage and then decreased as the damage was repaired (Figure 2I). Silencing *DDGC* or *RAD51* extended the time for repairing camptothecin-induced DSB in KGN cells as expected (Figure 2I), which further demonstrated that the HR repair process was impaired in *DDGC*-silenced or *RAD51*-silenced cells. Collectively, our findings suggest that *RAD51* is the critical target gene through which *DDGC* participates in DNA damage repair processes in GCs.

DDGC is necessary for the stabilization of *RAD51* mRNA by serving as a sponge for *miR-589-5p*

DDGC was predominantly localized in the cytoplasm of KGN and SVOG cells (Figures 3A and 3B), implying that it might serve as a

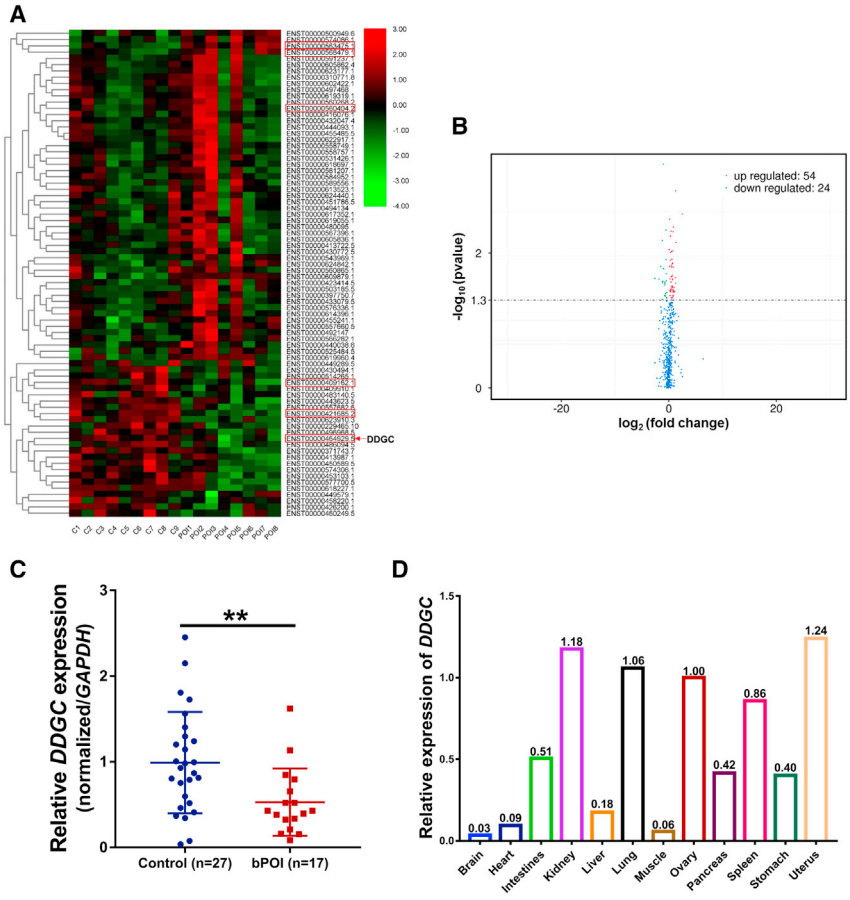

Figure 1. LncRNA *DDGC* is significantly minimally expressed in GCs from bPOI patients

(A) RNA-seq heatmap of lncRNAs with significantly altered expression in GCs from controls (n = 9) or bPOI patients (n = 8). LncRNAs selected for validation are marked by a red box. (B) Volcano plot showing the lncRNAs with significantly altered expression. (C) The qRT-PCR analysis of the expression levels of *DDGC* in GCs from controls (n = 27) or bPOI patients (n = 17). Error bars show the mean ± SD. **p < 0.01. (D) The qRT-PCR analysis of the expression levels of *DDGC* in 21-week fetal tissues. The expression level of *DDGC* in ovary was set to 1. *GAPDH* was regarded as an endogenous control for (C) and (D).

competitive endogenous RNA (ceRNA) by binding to microRNAs (miRNAs) and mediating mRNA degradation.[25] Cellular transcription and translation were inhibited by actinomycin D and cycloheximide, respectively. Then we conducted qRT-PCR and western blot assays to observe the degradation rate of *RAD51* mRNA and protein after *DDGC* knockdown. Results showed that silencing *DDGC* promoted the degradation of *RAD51* mRNA (Figure 3C), while the protein degradation rate remained unchanged compared with that of negative control cells (Figure 3D). Together, these results suggest that *DDGC* is necessary for *RAD51* mRNA stabilization rather than for degradation of RAD51 protein.

Table 2. Baseline characteristics of study participants for qRT-PCR

Characteristic	Control (n = 27)	bPOI (n = 17)	p
Age (years)	31.48 ± 3.96	32.65 ± 3.97	0.347[a]
BMI (kg/m^2)	21.85 ± 2.14	22.44 ± 3.76	0.510[a]
bFSH (IU/L)	6.31 ± 1.34	11.95 (11.33, 12.64)	<0.0001[b]
bLH (IU/L)	5.83 ± 1.51	5.76 ± 1.85	0.893[a]
bE2 (pg/mL)	36.11 ± 16.02	36.76 ± 17.04	0.898[a]
AMH (ng/mL)	3.21 ± 1.34	0.513 ± 0.30	<0.0001[a]

bFSH, basal FSH; bLH, basal luteinizing hormone; bE2, basal estradiol.
Data are presented as mean ± SD.
[a]Students' t test. Data are presented as median (interquartile range).
[b]Mann-Whitney U test.

Because argonaute RISC catalytic component 2 protein (Ago2) is a central element of the RNA-induced silencing complex involved in miRNA-regulated mRNA instability, we performed RNA immunoprecipitation (RIP) assays utilizing anti-Ago2 antibody and found that endogenous *DDGC* was preferentially co-precipitated by Ago2 compared with IgG (Figure 3E). Moreover, silencing of *RAD51* mRNA also reduced *DDGC* expression (Figure 3F). These results suggest that *DDGC* serves as a ceRNA to regulate *RAD51* mRNA stability and DNA damage repair.

Prediction using the publicly available starBase v.2.0 tool[26] showed that three miRNAs (*miR-384*, *miR-589-5p*, *miR-653-5p*) contained seed regions complementary to both *DDGC* and *RAD51* mRNA. Thus, we transfected KGN cells with mimics of the three candidate miRNAs, and the expression of lncRNAs *DDGC* and *RAD51* was detected via qRT-PCR and western blot. As shown in Figures 3G and 3H, both *miR-384* and *miR-589-5p* could downregulate the expression of *DDGC* and *RAD51* simultaneously. To further determine whether these two miRNAs bind to *DDGC* and *RAD51* mRNA, we established luciferase reporters comprising either wild-type (WT) or mutant (MT) *DDGC* or the 3′ UTR of *RAD51* mRNA (Figures S4A and S4B). As shown in Figures 3I and 3J, *miR-589-5p* overexpression significantly suppressed the luciferase activity of WT reporter vectors but not MT vectors in human embryonic kidney (HEK) 293 and HeLa cells. In contrast, *miR-384* mimics had no effect on either candidate target sequence (Figure S4C). Thus, we focused on *miR-589-5p* in seeking further evidence for this interaction. A biotin-labeled RNA pull-down assay showed that *miR-589-5p* precipitated endogenous *DDGC* and *RAD51* mRNA in KGN cells (Figure 3K). Moreover, *miR-589-5p* was pulled down by biotin-labeled antisense probes directed to *DDGC* (Figure 3L). These results indicate that *DDGC* directly "absorbs" *miR-589-5p* in order to regulate the stability of *RAD51* mRNA.

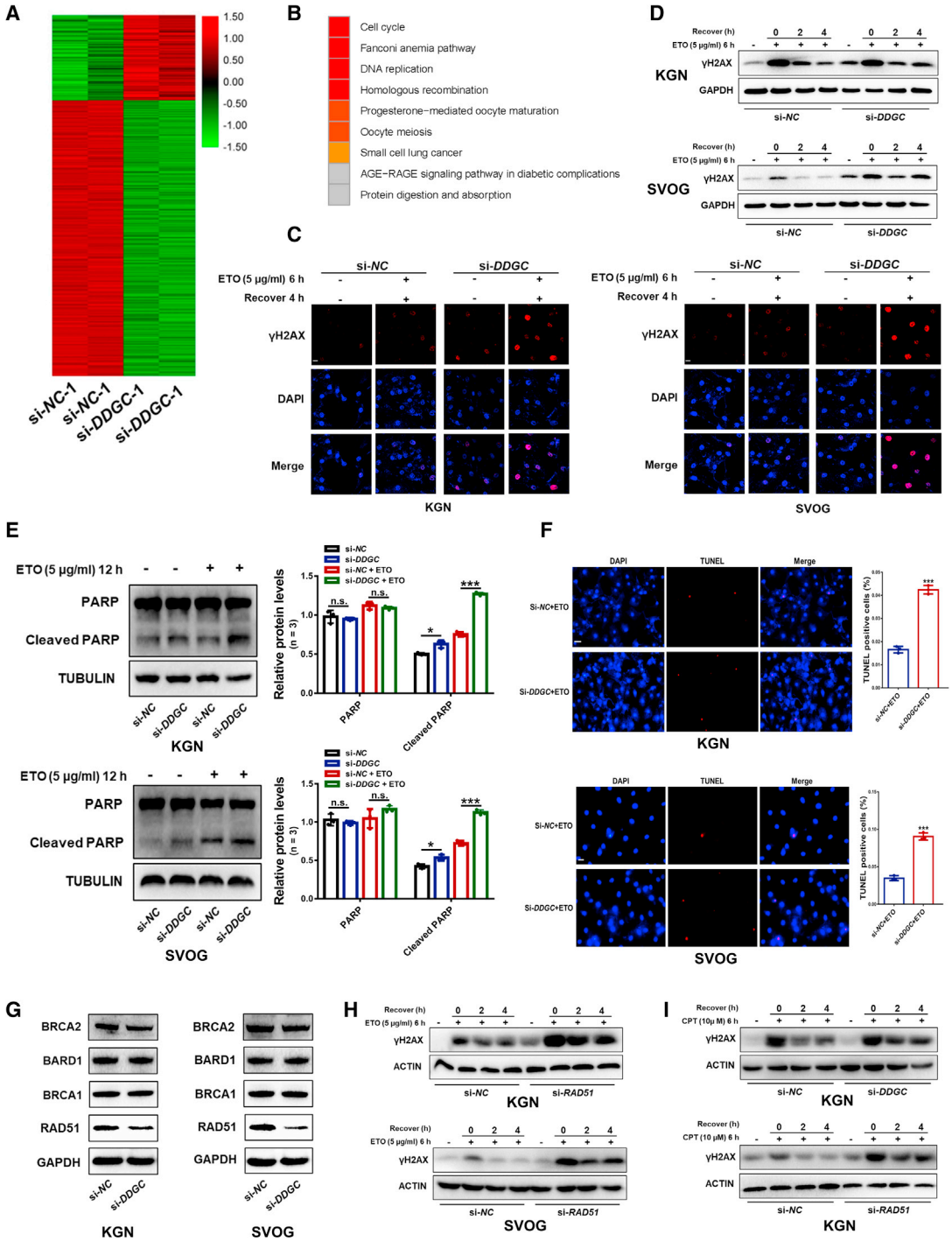

Figure 2. Silencing of *DDGC* impairs DNA damage repair through downregulation of *RAD51*

(A) RNA-sequencing heatmap of differentially expressed mRNAs between *DDGC*-silenced (n = 2) and negative control KGN cells (n = 2). (B) KEGG analysis of RNA-sequencing data for KGN cells after si-*DDGC* and si-*NC* transfection. (C) The etoposide (ETO)-induced γH2AX foci formation in KGN and SVOG cells after si-*DDGC* and si-*NC* transfection. Scale bars, 15 μm. (D) After exposure to ETO, the expression levels of γH2AX were measured by western blot in KGN and SVOG cells after si-*DDGC* and si-*NC* transfection. (E) The levels of cleaved PARP induced by ETO were measured by western blot in KGN and SVOG cells after si-*DDGC* and si-*NC* transfection. Protein levels were quantified by ImageJ software and normalized to the loading controls. Error bars show the mean ± SD from three repeated experiments. n.s., not significant; *$p < 0.05$, ***$p < 0.001$. (F) TUNEL assays of KGN and SVOG cells with si-*DDGC* and si-*NC* transfection, followed by the addition of ETO for 12 h. Error bars show the mean ± SD

(legend continued on next page)

Silencing of *DDGC* leads to the aberrant differentiation of GCs by downregulating *WT1*

Steroid hormone synthesis is indispensable for folliculogenesis, especially the conversion of androgen to estradiol, which is a characteristic of differentiated GCs.[27] Therefore, we further explored whether *DDGC* participated in estradiol synthesis. Interestingly, we found that the level of estradiol was significantly increased after *DDGC* silencing (Figure 4A), as were the markers of GC differentiation, i.e., FSHR and CYP19A1 (Figures 4B and 4C). In addition, genes that are involved in steroid hormone synthesis and GC differentiation were also found to be differentially expressed in the KGN RNA-seq analysis (GSE158555). These findings suggest that the aberrant differentiation of GCs can be attributed to *DDGC* silencing.

Because forkhead box O1 (*FOXO1*) and *WT1* are two critical transcription factors governing GC differentiation, we explored whether *FOXO1* and *WT1* were involved in the *DDGC* silencing-mediated aberrant differentiation of GCs. Intriguingly, WT1, but not FOXO1, was significantly downregulated after *DDGC* silencing (Figure 4D). Moreover, silencing *WT1* resulted in an apparent increased level of estradiol and expression of FSHR and CYP19A1 (Figures S4D, 4E, and 4F), which mimicked the results of *DDGC* silencing. In contrast, overexpression of *WT1* led to a significant decline in the levels of estradiol and FSHR and CYP19A1 expression, which partially rescued the impact of *DDGC* silencing on GC differentiation (Figures S4D, 4E, and 4F). In general, these data suggest that the aberrant differentiation of GCs after *DDGC* silencing can be attributed to insufficient *WT1* expression.

DDGC combines with HSP90 and mediates the degradation of the WT1 protein

To elucidate the mechanism through which *DDGC* silencing leads to decreased *WT1* expression, we observed the changes in WT1 protein and mRNA after *DDGC* silencing. The WT1 protein was notably diminished, whereas the level of *WT1* mRNA was not significantly changed (Figure 5A), which indicated that *DDGC* might regulate *WT1* mRNA translation or protein degradation. As shown in Figure 5B, treatment of cells with cycloheximide after *DDGC* silencing resulted in a notably shorter half-life of WT1 protein compared with controls, which suggested that *DDGC* mediates the degradation of WT1 protein. In addition to this, chloroquine and MG132 were used to block the autophagy and proteasome pathways in GCs, respectively. As shown in Figure 5C, treatment of cells with MG132 resulted in increased levels of endogenous WT1 protein compared with control cells, whereas chloroquine treatment had no impact on the decreasing level of WT1 protein upon *DDGC* knockdown (Figure S4E), thus indicating that *DDGC* modulates WT1 protein via the ubiquitin-proteasome pathway but not through autophagy. Indeed, the ubiquitination of the WT1 protein was dramatically increased in *DDGC*-silenced cells (Figure 5D). In summary, silencing of *DDGC* led to aberrant differentiation of GCs by promoting the ubiquitination and subsequent degradation of WT1.

Because the chaperone activity of HSP90 is essential for WT1 protein stability,[28] we focused on HSP90 to elucidate the possible mechanism underlying the *DDGC*-mediated ubiquitination of WT1. Consistent with the results presented above, diminished WT1 protein was observed in KGN cells treated with the HSP90 inhibitor 17-AAG, which could be rescued by MG132 (Figure 5E), indicating that inhibition of HSP90 chaperone activity promotes the ubiquitin-proteasome degradation of WT1 in GCs. As a molecular chaperone, HSP90 interacts with hundreds of proteins to help maintain their activity.[29] Therefore, we hypothesized that *DDGC* might act as an intermediate in the interaction between HSP90 and WT1. Intriguingly, immunofluorescence showed that HSP90 and WT1 were co-distributed in the nuclei of KGN cells (Figure S4F). *DDGC* silencing had no impact on the expression of HSP90 (Figure S4G); however, it impaired the interaction between HSP90 and WT1 in both nucleus and cytoplasm (Figure 5F). Together, these results suggest that *DDGC* mediates the interaction between HSP90 and WT1.

We further explored whether *DDGC* could directly bind to HSP90. The biotin-labeled RNA pull-down assay and subsequent western blot showed that HSP90 bound directly to *DDGC*, but not to *DDGC*-AS (Figure 5G). Furthermore, the RIP assay indicated an endogenous interaction between *DDGC* and HSP90 in KGN cells (Figure 5H). Collectively, these results suggest that *DDGC* is essential for the HSP90-WT1 interaction, and when *DDGC* is downregulated, HSP90 can no longer efficiently bind to WT1, leading to subsequent WT1 degradation.

DDGC regulates the expression of *Rad51* and DNA damage repair *in vivo*

To further verify the regulatory role of *DDGC* on the expression of *RAD51* and *WT1*, *DDGC* was introduced into *in vitro*-cultured mouse ovaries (Figure S4H) by infection or mouse ovaries (*in vivo*) by ovarian bursa injection with adenovirus expressing *DDGC* (Figure 6A). Results showed that overexpressing *DDGC* significantly decreased the protein levels of ETO-induced γH2AX and cleaved PARP in *in vitro*-cultured ovaries (Figure 6B); however, it had no impact on the ubiquitination of WT1 (Figure S4I). *In vivo* experiments found that the mRNA and protein levels of *Rad51* were significantly increased in ovaries overexpressing *DDGC* (Figures 6C and 6D), indicating the regulation of *DDGC* on *Rad51* expression *in vivo*. Meanwhile, no significant change was observed in the protein levels of WT1, FSHR, and CYP19A1 after *DDGC* overexpression (Figure S4J). The above-mentioned results suggested the protective role of *DDGC* in mouse ovaries upon DNA damage. Then, we explored the

from three repeated experiments. ***$p < 0.001$. Scale bars, 50 μm (KGN) or 20 μm (SVOG). (G) Western blots of protein levels of several essential genes related to DNA damage repair in KGN and SVOG cells after si-*DDGC* and si-*NC* transfection. (H) Western blots of protein levels of γH2AX in KGN and SVOG cells with si-*RAD51* and si-*NC* transfection after ETO exposure. (I) After exposure to camptothecin (CPT), the γH2AX levels were measured by western blot in si-*DDGC*-, si-*RAD51*-, and si-*NC*-transfected KGN cells.

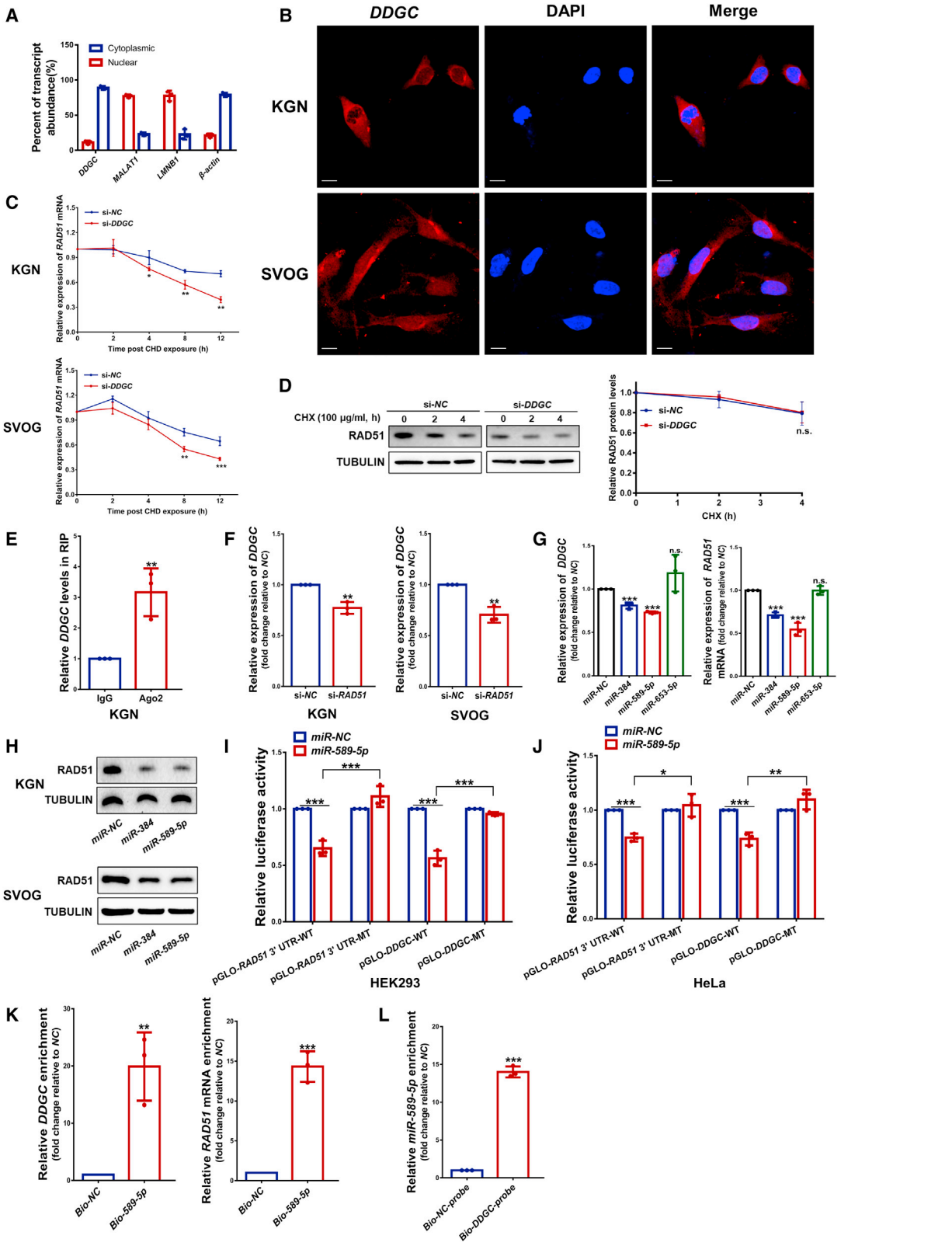

(legend on next page)

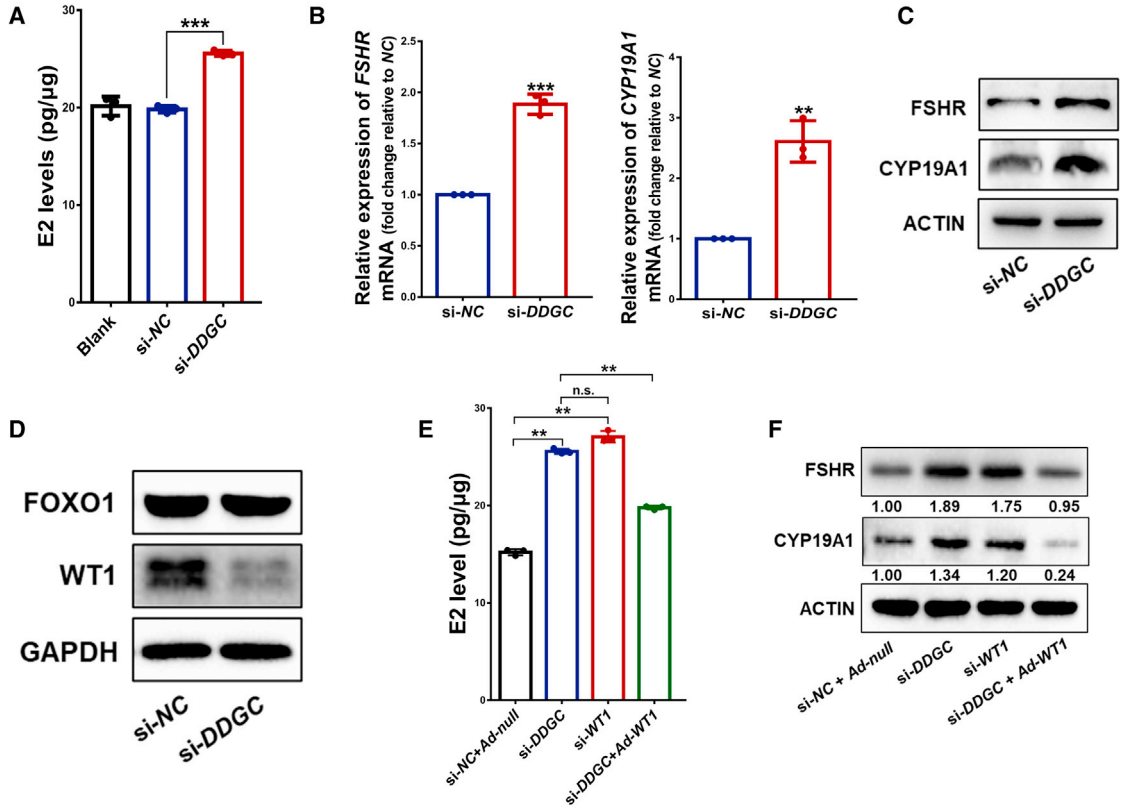

Figure 4. Silencing of *DDGC* leads to the aberrant differentiation of GCs through downregulation of *WT1*

(A) The estradiol (E2) level in the supernatant of KGN cells was measured after si-*DDGC* and si-*NC* transfection. Error bars show the mean ± SD from three repeated experiments. ***p < 0.001. (B) The qRT-PCR analysis of relative mRNA levels of *FSHR* and *CYP19A1* in KGN cells with si-*DDGC* and si-*NC* transfection. The qRT-PCR values were obtained from three repeated experiments. Error bars show the mean ± SD. **p < 0.01, ***p < 0.001. (C) The protein levels of FSHR and CYP19A1 in si-*DDGC*- and si-*NC*-transfected KGN cells were measured by western blot. (D) The protein levels of FOXO1 and WT1 in si-*DDGC*- and si-*NC*-transfected KGN cells were measured by western blot. (E) The estradiol levels were measured in negative control, *DDGC*-silenced, *WT1*-silenced, and co-transfected KGN cells. Error bars show the mean ± SD from three repeated experiments. n.s., not significant; **p < 0.01. (F) The protein levels of FSHR and CYP19A1 in negative control, *DDGC*-silenced, *WT1*-silenced, and co-transfected KGN cells were measured by western blot.

therapeutic effect of *DDGC* within mouse ovaries. After intraperitoneal injection of ETO, lower γH2AX and cleaved PARP protein levels, as well as TUNEL signals, were detected in ovaries overexpressing *DDGC* (Figures 6E and 6F). These data indicate the therapeutic effect of *DDGC* in mouse ovaries bearing DNA damage.

DISCUSSION

In the ovary, the roles and mechanisms of lncRNAs have not been extensively explored until recently. The latest reports have shown a relationship between certain lncRNAs and PCOS; for instance, *LINC-01572:28* and *Lnc-OC1* participate in PCOS development by

Figure 3. *DDGC* is necessary for the stabilization of *RAD51* mRNA by serving as a sponge for *miR-589-5p*

(A) The qRT-PCR analysis of the expression levels of *DDGC* in the cytoplasm and nucleus of KGN cells. *MALAT1* served as the cytoplasmic reference for lncRNA, and *lamin B1* and *β-actin* were used as the nuclear and cytoplasmic reference, respectively. (B) RNA fluorescence *in situ* hybridization (FISH) assay showing the subcellular localization of *DDGC* in KGN and SVOG cells. Scale bars, 10 μm. (C) *RAD51* mRNA expression in si-*DDGC*- and si-*NC*-transfected KGN and SVOG cells was measured by qRT-PCR at different time points after the addition of actinomycin D (CHD). (D) Western blots of the RAD51 protein levels in si-*DDGC*- and si-*NC*-transfected KGN cells at different time points after the addition of cycloheximide (CHX). Protein levels of RAD51 were quantified by ImageJ software and normalized to the loading controls. Error bars show the mean ± SD from three repeated experiments. (E) RIP assay of the enrichment of *DDGC* after anti-Ago2 immunoprecipitation. (F) The relative expression of *DDGC* in si-*RAD51*- and si-*NC*-transfected KGN and SVOG cells was measured by qRT-PCR. (G) qRT-PCR was applied to analyze the relative expression levels of *DDGC* and *RAD51* mRNA in miRNA mimics and negative-control-transfected KGN cells. (H) Western blots of the RAD51 protein levels in miRNA-mimics and negative-control-transfected KGN and SVOG cells. (I, J) Luciferase activities were analyzed at 48 h after co-transfection of reporter vectors and *miR-589-5p* or negative control in (I) HEK293 or (J) HeLa cells. Data are presented as the mean ± SD from three repeated experiments. (K) Enrichment of *DDGC* and *RAD51* after biotin-*miR-589-5p* or biotin-negative control pull-down. (L) Enrichment of *miR-589-5p* pulled down by biotin-labeled probes directed to *DDGC* and biotin-labeled negative control probes. Error bars show the mean ± SD. The qRT-PCR values in (A), (C), (E–G), (K), and (L) were obtained from three repeated experiments. n.s., not significant; *p < 0.05, **p < 0.01, ***p < 0.001.

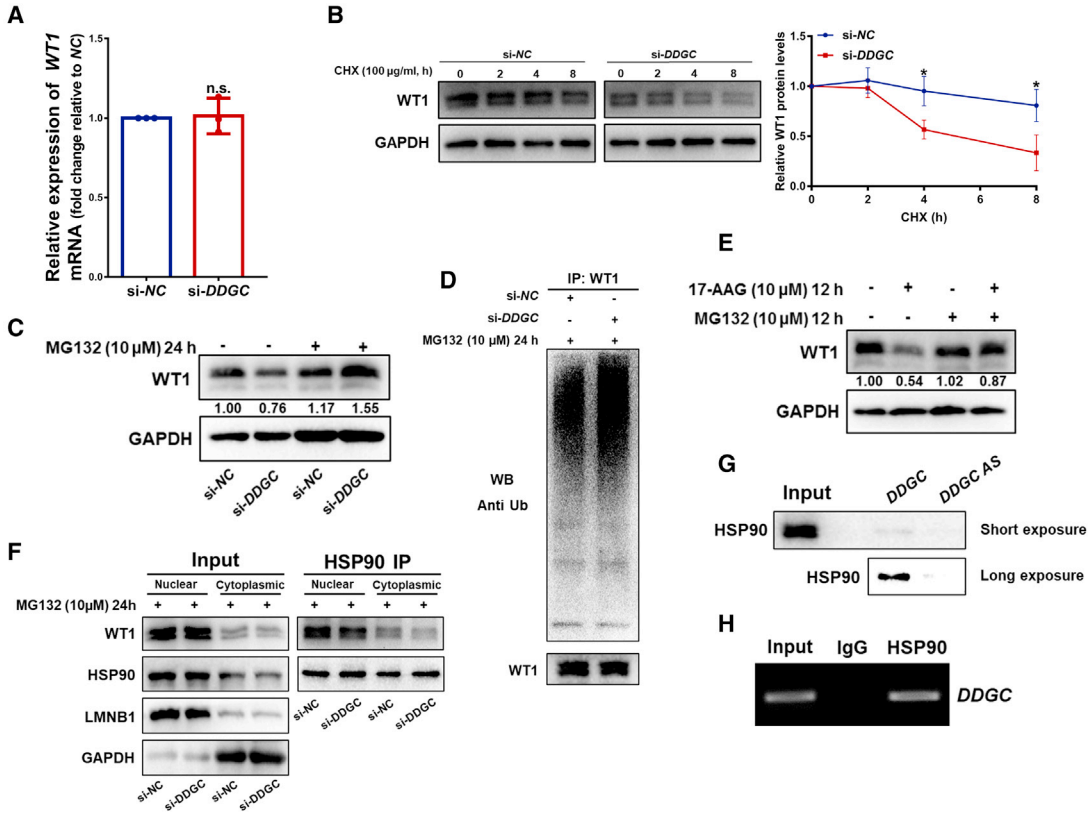

Figure 5. *DDGC* combines with HSP90 and mediates the degradation of the WT1 protein

(A) The qRT-PCR analysis of the relative *WT1* mRNA levels in si-*DDGC*- and si-*NC*-transfected KGN cells. The qRT-PCR values were obtained from three repeated experiments. Error bars show the mean ± SD. n.s., not significant. (B) Western blots of the WT1 protein levels in si-*DDGC*- and si-*NC*-transfected KGN cells at different time points after the addition of CHX. Protein levels of WT1 were quantified by ImageJ software and normalized to the loading controls. Error bars show the mean ± SD from three repeated experiments. *$p < 0.05$. (C) Western blots of protein levels of WT1 in KGN cells with si-*DDGC* or si-*NC* transfection, followed by the addition of MG132 for 24 h. (D) The polyubiquitination level of WT1 in si-*DDGC*- and si-*NC*-transfected KGN cells at 24 h after the addition of MG132 was measured by western blot. The bottom blot depicts the input of the cell lysates. (E) Western blots of protein levels of WT1 in KGN cells at 12 h after the addition of 17-AAG and MG132. (F) Western blots of protein levels of WT1 in si-*DDGC*- and si-*NC*-transfected KGN cells after anti-HSP90 immunoprecipitation. (G) Western blots of the proteins pulled down by biotin-labeled *DDGC* and *DDGC*-AS. (H) RIP assays were conducted using the anti-HSP90 antibodies in KGN cells, and RT-PCR was used to measure *DDGC*.

mediating GC proliferation.[17,30] However, few lncRNAs have been explored in POI pathogenesis. Here, we identified the lncRNA *DDGC*, which plays dual roles in both DNA damage repair progression and the differentiation of GCs. Our mechanistic study showed that *DDGC* modulated the stability of *RAD51* mRNA and WT1 protein simultaneously (Figure 7). Interestingly, a similar mode of action is seen for the lncRNAs *GUARDIN* and *OVAAL*, which have recently been identified to play dual roles in the senescence and survival of cancer cells.[31,32] The dual functions of these lncRNAs are carried out at the same time in a non-interfering manner, which provides deeper insights into their RNA regulatory effects. However, a lack of such molecules in GCs has impeded our understanding of the pathogenic mechanism behind the development of POI. Our findings are the first to show that *RAD51* and *WT1*, two pathogenic genes for POI, are post-transcriptionally modulated by lncRNA *DDGC* in GCs, providing new insights into the contribution of lncRNAs to POI pathogenesis.

In mammals, abnormal GC function contributes to follicle atresia and POI,[13] and if DSBs in GCs are not repaired correctly or promptly this can also lead to cell death and then atretic follicles and premature ovarian aging.[33,34] Variants within a series of DNA repair genes, such as *MCM8*,[35] *MSH5*,[36] and *BRCA2*,[37,38] have been proved as causative factors for POI. In addition, lncRNA *HCP5* was previously shown to participate in the development of POI by mediating the process of DNA damage repair in GCs.[39] In this study, our results show that downregulation of *DDGC* inhibited the DNA damage repair activity of GCs by degrading *RAD51* mRNA and impairing the HR pathway, thereby leading to GC apoptosis. Thus, our results shed new light on how lncRNAs regulate the process of DNA damage repair in GCs.

In the present study, we identified a ceRNA network through which lncRNA *DDGC* regulates the expression of the DNA repair gene *RAD51*. *RAD51* is the eukaryotic ortholog of the bacterial recombinase RecA, which plays a central role in the error-free HR pathway

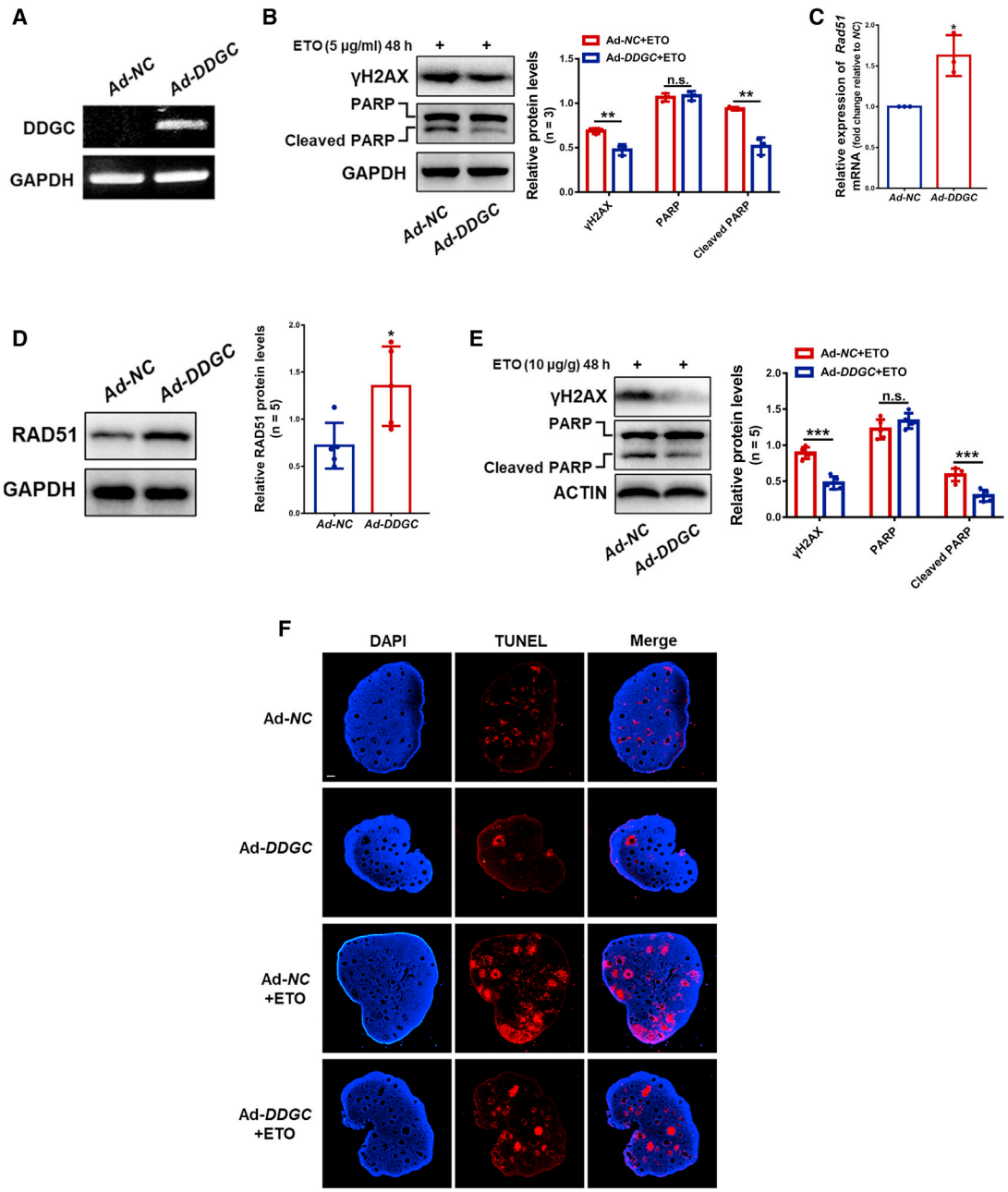

Figure 6. *DDGC* regulates the expression of *Rad51* and DNA damage repair *in vivo*

(A) The RT-PCR analysis of the expression of *DDGC* in mouse ovaries infected with adenovirus. (B) The protein levels of γH2AX and cleaved PARP in *DDGC*-overexpressing and negative control *in vitro*-cultured ovaries were measured by western blot at 48 h after the addition of ETO. (C) The qRT-PCR analysis of the relative mRNA levels of *Rad51* in *DDGC*-overexpressing and negative control mouse ovaries. The qRT-PCR values were obtained from three repeated experiments. Error bars show the mean ± SD. (D) Western blots of the protein levels of RAD51 in *DDGC*-overexpressing and negative control mouse ovaries. (E) Western blots of the protein levels of γH2AX and cleaved PARP in *DDGC*-overexpressing and negative control mouse ovaries at 48 h after the addition of ETO. (F) The apoptosis of *DDGC*-overexpressing and negative control mouse ovaries at 48 h after the addition of ETO was measured by TUNEL assay. Scale bar, 100 μm. Error bars show the mean ± SD. Protein levels of (B), (D), and (E) were quantified by ImageJ software and normalized to the loading controls. n.s., not significant; *$p < 0.05$, **$p < 0.01$, ***$p < 0.001$.

of DNA repair.[40,41] The latest studies have shown that *Rad51*-mediated HR is the predominant pathway in oocytes for repairing DSBs,[42] especially in primordial follicles.[43] Furthermore, through whole-exome sequencing, a pathogenic variant of *RAD51* has been identified in POI patients with primary amenorrhea.[44] Consistent with this, our results show the impact of dysregulated *RAD51* on

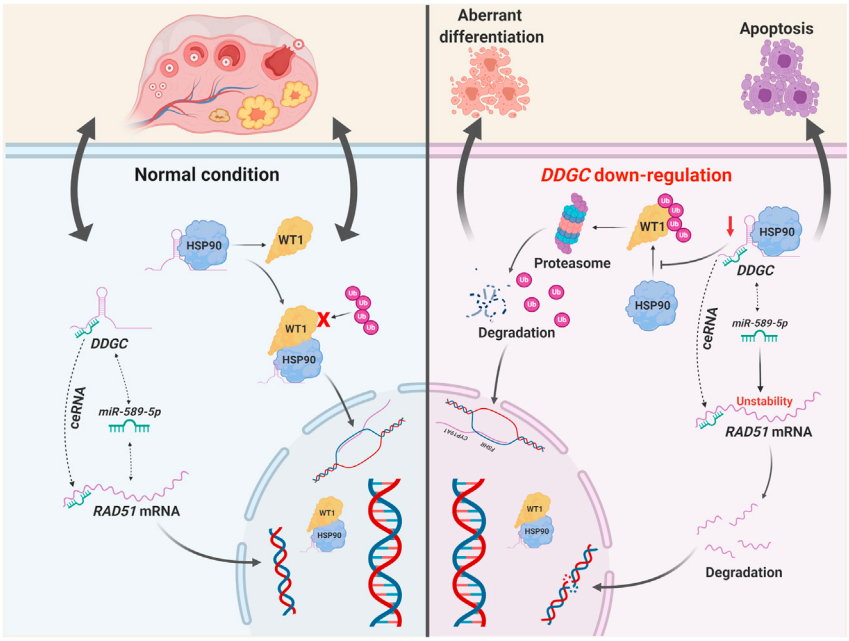

Figure 7. The schematic model for the post-transcriptional regulation and function of lncRNA *DDGC*

GC function and survival, not only strengthening the role of DNA repair deficiency in the pathogenesis of POI, but also highlighting *DDGC* as an important modulator of *RAD51*. To our knowledge, this is the first report of a ceRNA mechanism involved in POI pathogenesis.

The second mechanism through which silencing of *DDGC* interferes with GC function is the accelerated degradation of the WT1 protein by binding to HSP90, and this leads to aberrant GC differentiation. *WT1* is a known causative gene for POI[16,45] due to its role in regulating genes responsible for GC differentiation, including *SF1*, *FSHR*, and *CYP19A1*.[45,46] However, the post-transcriptional regulation of *WT1* in the ovary has not been previously described. We show here that the chaperone activity of HSP90 governs the stability of the WT1 protein in GCs. In addition, we show the essential role of *DDGC* in the HSP90-WT1 interaction, thereby protecting the WT1 protein from ubiquitin-mediated protein degradation. Similarly, lncRNA *GLCC1* and *GALNT5* UTR-associated RNA have been reported to interact with HSP90 and to mediate the ubiquitination of substrate proteins such as c-Myc and IKK in colorectal cancer and gastric cancer.[47,48] We have identified *DDGC* as a novel regulator of WT1 ubiquitination by binding to HSP90 in GCs, suggesting the protein binding domain within *DDGC*. Based on the current findings, it is reasonable to hypothesize that lncRNA *DDGC* might maintain the efficient combination of HSP90 and WT1 through the secondary structure formed by itself. Spatial structure is an essential feature of non-coding RNAs and is closely related to cellular conditions and processes, such as capping, splicing, polyadenylation, and folding.[49,50] For example, the lncRNA *HOTAIR* tethers multiple histone-modifying complexes through its intricate secondary structure.[51,52] However, inappropriate modification could be made by endonucleases and spliceosomes in mouse GCs due to the low conservative property of the *DDGC* sequence, resulting in incorrect folding and inaccurate structure formation. In the present study, protein levels of WT1 remain unchanged upon *DDGC* overexpression *in vivo*, which might be because *DDGC* of adenovirus origin could not form the homologous spatial structure in mouse ovaries. Further studies are warranted to elucidate the physiological role of *DDGC in vivo* and whether this lncRNA-protein regulatory mechanism exists in mouse GCs.

In summary, we have demonstrated here that lncRNA *DDGC* participates in POI pathogenesis by post-transcriptionally regulating the stability of *RAD51* mRNA and WT1 protein. In particular, our study has expanded on the two regulatory mechanisms of lncRNAs in POI, and we propose a new epigenetic mechanism in the etiology of POI in which the two causative genes, *RAD51* and *WT1*, are regulated simultaneously. Therefore, *DDGC* might be a potential therapeutic approach for POI.

MATERIALS AND METHODS

Clinical samples

The participants in this study were recruited from the Reproductive Hospital affiliated with Shandong University after written informed consent was obtained. The groups contained 25 bPOI patients and 36 age and BMI-matched healthy women (control group). All of the participants were undergoing *in vitro* fertilization or intracytoplasmic sperm injection and embryo transfer (IVF/ICSI-ET) treatment because of tubal or male factors. The bPOI patients were recruited according to the following criteria: (1) <40 years of age; (2) menstrual cycle 23–35 days; (3) basal follicle-stimulating hormone (bFSH) 10 < serum bFSH < 25 (IU/L); (4) serum anti-Müllerian hormone (AMH) <1.1 ng/mL. Women with chromosomal abnormalities or carrying POI-causative mutations, or with an experience of ovarian radiotherapy, chemotherapy, or surgery, were precluded. The study was under approval from the Institutional Review Board (IRB) of Reproductive Medicine of Shandong University. The clinical indicators of all participants are summarized in Tables 1 and 2. GCs were collected from participants and prepared as previously described.[39]

RNA-seq analysis

The total RNA was purified from the GCs of eight bPOI patients and nine controls utilizing the TRIzol reagent (TaKaRa, China). The degradation, contamination, purity, concentration, and integrity of

total RNA were monitored by agarose gels, spectrophotometer instruments (IMPLEN, USA), a Qubit RNA detection kit (Life Technologies, USA), and an RNA Nano 6000 Assay Kit (Agilent Technologies, USA). The input RNA for sample preparations was set as 3 μg RNA per sample. An rRNA Removal Kit (Epicentre, USA) and subsequent ethanol precipitation were utilized to remove rRNA. Subsequently, the rRNA-free RNA was used to generate the libraries for sequencing using a NEBNext Ultra Directional RNA Library Prep Kit for Illumina (NEB, USA) according to the manufacturer's instructions. An AMPure XP system (Beckman Coulter, Beverly, MA, USA) was utilized to purify the library fragments and subsequently collect cDNA fragments with length ranging from 150 to 200 bp. The generation of the cluster was conducted via the TruSeq PE Cluster Kit v.3-cBot-HS (Illumina) following the manufacturer's guidelines. Then, the sequencing was performed on the Illumina HiSeq 4000 platform with 150-bp paired-end reads generated. Low-quality reads, as well as reads containing adapter and poly-N, were removed, thereby generating clean reads. Coding potential analysis was performed utilizing CNCI, CPC, Pfam-sca, and phyloCSF software. The Cuffdiff (v.2.1.1) was applied to calculate the fragments per kilobase of transcript per million mapped reads (FPKMs) of both lncRNAs and mRNAs in each sample. Differentially expressed transcripts were assigned as p-adjust <0.05. Significantly enriched gene ontology (GO) terms were assigned as $p < 0.05$. Significantly enriched KEGG pathways were determined by KOBAS software. The raw data have been uploaded as GEO: GSE158526.

For KGN RNA-seq analysis, the total RNA was extracted from KGN cells at 48 h after transfection with *DDGC* siRNA (si-*DDGC*) or with negative control siRNA (si-*NC*). RNA-seq and data analyses were carried out by Annoroad (China). A Kaiao K5500 spectrophotometer (Kaiao, China) was used to check the purity of total RNA. The input RNA for sample preparations was set as 2 μg RNA per sample. The library RNA concentration was diluted to 1 ng/μL after quantification using a Qubit RNA Assay Kit in Qubit 3.0. The Agilent Bioanalyzer 2100 system (Agilent Technologies) and StepOnePlus Real-Time PCR System were utilized to quantify the insert size. The cluster was generated via HiSeq PE Cluster Kit v.4-cBot-HS (Illumina) following the manufacturer's guidelines. Subsequently, the sequencing was conducted on an Illumina platform. The remaining steps were the same as in the above paragraph. The raw data have been uploaded as GEO: GSE158555.

Isolation of RNA and qRT-PCR assays

The expression of *DDGC* in GCs was validated from an independent cohort consisting of 17 bPOI patients and 27 controls. The extraction of RNA from GCs or cell lines was conducted according to protocols as described above. The PrimeScript RT Reagent Kit (TaKaRa) was utilized to reverse transcribe all mRNAs and lncRNAs, whereas miRNA-specific reverse transcription primers (GenePharma, China) were used to reverse transcribe miRNAs individually. The SYBR Green Master Mix (TaKaRa) was applied for quantitative RT-PCR, and *GAPDH* was regarded as an endogenous control for qRT-PCR of mRNAs and lncRNAs. *U6* was regarded as an endogenous control for qRT-PCR of miRNAs. The qRT-PCR assay per sample was run in triplicate, and the $2^{-\Delta\Delta Ct}$ method was applied to analyze all obtained values. Table S2 shows the primers used for qRT-PCR analysis.

Cell lines, cell culture, and transfection of vectors

The KGN GC tumor cell line was purchased from RIKEN BRC (Japan).[53] SVOG (luteinized GC line) was generously provided by Professor Peter C.K. Leung. The culture medium was prepared, to which 10% fetal bovine serum (FBS) (Gibco, USA) and 1% penicillin/streptomycin (P/S) (Invitrogen, USA) were added. KGN and SVOG cells were grown in DMEM/F12 culture medium (HyClone, USA), and the HEK293 and HeLa (human cervix carcinoma) cells were cultured in DMEM high-glucose culture medium (HyClone). All cells were incubated under humid conditions at 37°C and 5% CO_2.

The siRNA duplexes and miRNA mimics applied in this study were generated at GenePharma. The cDNA sequence encoding human *RAD51* was subcloned into the pEGFP-N1 vector (*pEGFP-N1-RAD51*), and an empty vector served as the control (*pEGFP-N1*). Adenoviruses for overexpressing *WT1* (Ad-*WT1*) were designed by Cyagen (China). The virus that expresses only GFP was regarded as a negative control (Ad-*null*) and cells were infected with 1×10^6 PFU/mL for the *in vitro* experiments. Transfection of siRNA duplexes, pEGFP-N1 vectors, and miRNA mimics was conducted using the Lipofectamine 3000 reagent (Invitrogen) following the manufacturer's protocols. Downstream experiments were conducted 48 h after transfection or infection. Table S3 shows the sequences of all siRNAs involved in this study.

CCK8 assay

KGN cells were seeded onto 96-well dishes at a density of 4,000 cells/well. Cell Counting Kit-8 (CCK8, Beyotime, China) was used to measure the viability of KGN cells at different times after transfection.

EdU assay

KGN cells were seeded onto 96-well plates and fixed at 48 h after transfection. Then, a cell proliferation assay (EdU, RiboBio, China) was performed in triplicate following the manufacturer's protocols.

Cell-cycle analysis by flow cytometry

KGN cells were cultured in 10-cm^2 plates and collected at 48 h after transfection. Then, 70% prechilled ethanol was utilized to fix cells at 4°C for 2 h. Subsequently, cells were stained with 7-AAD (Multi Sciences, China) followed by flow cytometry cell-cycle analysis.

Western blot

Cell pellets were lysed by SDS or RIPA solution incorporating an inhibitor of proteinase (Cell Signaling Technology, USA), and total protein was extracted immediately following the manufacturer's instructions. Approximately 20 μg of protein was loaded and separated on NuPAGE bis-tris mini gels (Invitrogen) or SDS polyacrylamide gels and subsequently transferred onto polyvinylidene fluoride (PVDF) membranes (Millipore, USA). Then, the PVDF membranes were blocked after treatment with 5% non-fat milk at room temperature

for 1 h. Blocked membranes were mixed with a solution of specific primary antibodies at 4°C overnight. Subsequently, secondary antibodies (Proteintech, China) were added and reacted with the primary antibodies at room temperature for 1 h. After staining via ECL chemiluminescence kit (Millipore), protein bands were detected by a ChemiDoc MP imaging system (Bio-Rad, USA). Table S4 shows the antibodies used for western blot.

DNA damage assay

KGN and SVOG cells were cultured in 12-well plates. Cells were harvested immediately at 48 h after transfection, or were exposed to 5 μg/mL ETO or 10 μM camptothecin for 6 h, followed by recovery for 2 or 4 h. The expression of the DNA damage marker γH2AX was measured by western blot.

Immunofluorescence

KGN and SVOG cells were fixed by treatment with paraformaldehyde at a concentration of 4% at 37°C for 20 min. Permeabilization and blocking were accomplished after treatment with 0.3% Triton X-100 and 10% BSA at room temperature for 30 min. The samples were incubated at 4°C overnight with specific primary antibodies. Subsequently, the antibodies were labeled at room temperature through treatment with Alexa Fluor secondary antibody for 1 h. Nuclei were stained with DAPI. A laser confocal microscope (ANDOR, UK) was utilized to capture images. Table S4 shows the antibodies used for immunofluorescence.

Terminal deoxynucleotidyl transferase dUTP nick-end labeling assays

At 48 h after transfection, ETO was added to the culture medium of KGN and SVOG cells at a concentration of 5 μg/mL for 12 h to induce DNA damage, followed by TUNEL assays using a TUNEL kit (KeyGen, China) following the manufacturer's protocols.

Nuclear and cytoplasmic component separation

The nuclear and cytoplasmic components were isolated via the PARIS™ Kit (Invitrogen) following the manufacturer's protocols. After purification, proteins or RNAs were subjected to western blot or qRT-PCR analysis. For qRT-PCR analysis, the input RNA was set at 100% to normalize the expression levels of *DDGC* along with the reference genes in the cytoplasmic and nuclear fractions.

Fluorescence *in situ* hybridization

DDGC probes were synthesized by RiboBio and labeled with Cy3. Then, assays were conducted using a fluorescence *in situ* hybridization (FISH) kit (RiboBio) following the manufacturer's protocols. The samples were observed using a laser confocal microscope (ANDOR, UK).

Actinomycin D exposure

KGN and SVOG cells were cultured in 12-well plates. At 24 h after transfection, cellular transcription was blocked for 0, 2, 4, 8, or 12 h through the addition of actinomycin D to the culture medium at the final concentration of 10 μM. The qRT-PCR assay was performed to measure RAD51 mRNA expression levels.

Cycloheximide exposure

KGN cells were cultured in 12-well plates. At 24 h after transfection, cellular translation was blocked for 0, 2, or 4 h through the addition of cycloheximide to the culture medium at the final concentration of 100 μg/mL. Cells were harvested and the proteins were analyzed by western blot.

RNA immunoprecipitation

RIP assays were carried out using the EZ-Magna RIP kit (Millipore) following the manufacturer's protocols. The cells (10^7 per sample) were lysed by RIP lysis solution containing inhibitors of RNase and protease. After one period of freezing and melting, specific primary antibodies or homologous IgG (negative control) was added to cell lysates and incubated overnight at 4°C. TRIzol reagent and subsequent qRT-PCR were used to extract and quantify the immunoprecipitated RNA as described above. The antibodies used for RIP assays are listed in Table S4.

Dual luciferase reporter assay

The pmirGLO plasmids containing approximately 150 bp of *RAD51* mRNA 3′ UTR or *DDGC* sequences with WT or deleted miRNA binding sites were generated and purchased from Promega (Madison, WI, USA). Plasmids and miRNA mimics or negative controls were co-introduced into HEK293 or HeLa cells. At 48 h after transfection, the cells were lysed and the luciferase activity of HEK293 or HeLa cells was assessed based on the protocols of the Dual-Luciferase Reporter Assay System (Promega).

Biotin-labeled RNA pull-down assay

For the biotin-labeled miRNA pull-down assays, *bio-589-5p* (biotin-labeled *miR-589-5p*) or *bio-NC* (empty vector) was designed by GenePharma and subsequently introduced into KGN cells. Cells were lysed followed by incubation with Pierce IP lysis buffer (Invitrogen) supplemented with inhibitors of protease and RNase. For the *DDGC* pull-down assay, KGN cells were lysed followed by incubation with the biotinylated *DDGC* probe (*Bio-DDGC-probe*) or negative control probe (*Bio-NC-probe*) or with the *in vitro*-transcribed *DDGC* sense strand and anti-sense strand (*DDGC*-AS). *In vitro* transcription was performed to generate biotin-labeled RNA via the MEGAscript T7 transcription kit (Invitrogen). Then magnetic streptavidin beads (Invitrogen) were added to the cell lysates, followed by incubation with RNA capture buffer at room temperature for 2 h. TRIzol reagent and qRT-PCR were used to isolate and quantify the RNA bound to the beads. Co-precipitated proteins were analyzed by western blot.

Detection of estradiol

KGN cells were cultured in 12-well plates. The KGN cell culture medium was replaced with DMEM without phenol red at 48 h after transfection, followed by treatment with 10 nM androstenedione

for 24 h. The Roche Cobas e 801 system was used to determine the concentration of estradiol from the supernatant.

Chloroquine and MG132 exposure

KGN cells were cultured and transfected in 12-well plates. Subsequently, the cellular pathway of autophagy or proteasome was blocked through treatment with 50 μM chloroquine or 10 μM MG132 for 24 h, respectively. Then, the cells were harvested and the proteins were analyzed by western blot.

Co-immunoprecipitation and ubiquitination assay

KGN cells were harvested with Pierce IP lysis buffer containing proteinase protease. Proteins were extracted and subsequently treated with the specific primary antibodies at 4°C overnight. Pure-Proteome Protein A/G magnetic beads (Millipore) were applied to precipitate the proteins at room temperature for 1 h. Loading buffer was used to resuspend the reaction mixtures after immunoprecipitation. Immunoprecipitated proteins were denatured and further analyzed by western blot. Table S4 shows the antibodies for co-immunoprecipitation.

17-AAG exposure

KGN cells were cultured in 12-well plates, followed by exposure to 10 μM 17-AAG alone or combined with 10 μM MG132 for 12 h, and the cells were harvested and the proteins were analyzed by western blot.

Ovary culture *in vitro*

All experiments involving mice were approved by the IRB of Reproductive Medicine of Shandong University and conformed to NIH regulatory standards. The *in vitro* culture system was established as previously described.[54] Briefly, 21-day-old female mice with C57BL/6 background were purchased from Charles River Laboratories (China) and sacrificed by cervical dislocation. After isolation by microdissection, mouse ovaries were cultured in six-well culture dishes (NEST, China) with a plate (Sigma, USA). The culture medium contained 1,200 μL DMEM/F12 (Gibco) plus 1 μg/μL AlbuMAX II (Gibco), 0.18% L-ascorbic acid (Sigma), 1% ITS (Sigma, USA), and penicillin/streptomycin. Ovaries were incubated under humidified conditions at 37°C and 5% CO_2. Adenoviruses for overexpressing *DDGC* (Ad-*DDGC*) and empty virus (Ad-*NC*) were synthesized by HanBio (China). A total of 1 μL Ad-*DDGC* or Ad-*NC* at 1×10^{11} PFU/mL was introduced into the medium. *In vitro*-cultured ovaries were harvested or treated with 5 μg/mL ETO or 10 μM MG132 at 48 h after infection, followed by H&E staining, co-immunoprecipitation, or western blot.

In vivo assays

A total of 10 μL Ad-*DDGC* or Ad-*NC* at 1×10^{11} PFU/mL was injected into 21-day-old female mouse ovarian bursa. Seven days after injection, the expression levels of RNA and protein were analyzed by RT-PCR and western blot. DNA damage was induced by intraperitoneal injection of ETO at 10 μg/g. The ovaries were harvested for western blot and TUNEL assay at 48 h after ETO injection. The TUNEL assays were performed using a TUNEL detection kit (KeyGen, China) following the manufacturer's protocols.

Statistics

All the statistical analyses were performed by SPSS software and GraphPad Prism 7 software. Except where indicated otherwise, the statistical significance was determined by the two-tailed Student t test. A $p < 0.05$ was considered statistically significant.

DATA AVAILABILITY

The data reported in this study have been deposited in GEO: GSE158526 (https://www.ncbi.nlm.nih.gov/geo/query/acc.cgi?acc=GSE158526) and GSE158555 (https://www.ncbi.nlm.nih.gov/geo/query/acc.cgi?acc=GSE158555).

SUPPLEMENTAL INFORMATION

Supplemental information can be found online at https://doi.org/10.1016/j.omtn.2021.10.015.

ACKNOWLEDGMENTS

This study was supported by the National Key Research & Developmental Program of China (2016YFC1000604, 2017YFC1001100). The authors thank all participants.

AUTHOR CONTRIBUTIONS

Y.Q. and S.Z. contributed to the study design and direction. X.W. and L.X. contributed to analysis and interpretation of the results. Y.D. participated in designing the experiment. P.C.K.L., G.L., and W.-Y.C. participated in providing the SVOG cell line. D.L. and W.X. contributed to the experiment completion and manuscript draft. All of the authors read, revised, and approved the final manuscript.

DECLARATION OF INTERESTS

The authors declare no competing interests.

REFERENCES

1. Djebali, S., Davis, C.A., Merkel, A., Dobin, A., Lassmann, T., Mortazavi, A., Tanzer, A., Lagarde, J., Lin, W., Schlesinger, F., et al. (2012). Landscape of transcription in human cells. Nature *489*, 101–108.
2. Deveson, I.W., Hardwick, S.A., Mercer, T.R., and Mattick, J.S. (2017). The dimensions, dynamics, and relevance of the mammalian noncoding transcriptome. Trends Genet. *33*, 464–478.
3. Kopp, F., and Mendell, J.T. (2018). Functional classification and experimental dissection of long noncoding RNAs. Cell *172*, 393–407.
4. Fatica, A., and Bozzoni, I. (2014). Long non-coding RNAs: new players in cell differentiation and development. Nat. Rev. Genet. *15*, 7–21.
5. Slack, F.J., and Chinnaiyan, A.M. (2019). The role of non-coding RNAs in oncology. Cell *179*, 1033–1055.
6. Atianand, M.K., Caffrey, D.R., and Fitzgerald, K.A. (2017). Immunobiology of long noncoding RNAs. Annu. Rev. Immunol. *35*, 177–198.
7. Poller, W., Dimmeler, S., Heymans, S., Zeller, T., Haas, J., Karakas, M., Leistner, D.M., Jakob, P., Nakagawa, S., Blankenberg, S., et al. (2018). Non-coding RNAs in cardiovascular diseases: diagnostic and therapeutic perspectives. Eur. Heart J. *39*, 2704–2716.
8. Coulam, C.B., Adamson, S.C., and Annegers, J.F. (1986). Incidence of premature ovarian failure. Obstet. Gynecol. *67*, 604–606.

9. European Society for Human, R.; Embryology Guideline Group on, POI., Webber, L., Davies, M., Anderson, R., Bartlett, J., Braat, D., Cartwright, B., Cifkova, R., de Muinck Keizer-Schrama, S., et al. (2016). ESHRE Guideline: management of women with premature ovarian insufficiency. Hum. Reprod. *31*, 926–937.
10. Qin, Y., Jiao, X., Simpson, J.L., and Chen, Z.J. (2015). Genetics of primary ovarian insufficiency: new developments and opportunities. Hum. Reprod. Update *21*, 787–808.
11. Robker, R.L., and Richards, J.S. (1998). Hormone-induced proliferation and differentiation of granulosa cells: a coordinated balance of the cell cycle regulators cyclin D2 and p27Kip1. Mol. Endocrinol. *12*, 924–940.
12. Zhou, J., Kumar, T.R., Matzuk, M.M., and Bondy, C. (1997). Insulin-like growth factor I regulates gonadotropin responsiveness in the murine ovary. Mol. Endocrinol. *11*, 1924–1933.
13. Matsuda, F., Inoue, N., Manabe, N., and Ohkura, S. (2012). Follicular growth and atresia in mammalian ovaries: regulation by survival and death of granulosa cells. J. Reprod. Dev. *58*, 44–50.
14. Di Pasquale, E., Beck-Peccoz, P., and Persani, L. (2004). Hypergonadotropic ovarian failure associated with an inherited mutation of human bone morphogenetic protein-15 (BMP15) gene. Am. J. Hum. Genet. *75*, 106–111.
15. Liu, H., Xu, X., Han, T., Yan, L., Cheng, L., Qin, Y., Liu, W., Zhao, S., and Chen, Z.J. (2017). A novel homozygous mutation in the FSHR gene is causative for primary ovarian insufficiency. Fertil. Steril *108*, 1050–1055.e1052.
16. Wang, H., Li, G., Zhang, J., Gao, F., Li, W., Qin, Y., and Chen, Z.J. (2015). Novel WT1 missense mutations in han Chinese women with premature ovarian failure. Sci. Rep. *5*, 13983.
17. Zhao, J., Xu, J., Wang, W., Zhao, H., Liu, H., Liu, X., Liu, J., Sun, Y., Dunaif, A., Du, Y., et al. (2018). Long non-coding RNA LINC-01572:28 inhibits granulosa cell growth via a decrease in p27 (Kip1) degradation in patients with polycystic ovary syndrome. EBioMedicine *36*, 526–538.
18. Che, Q., Liu, M., Zhang, D., Lu, Y., Xu, J., Lu, X., Cao, X., Liu, Y., Dong, X., and Liu, S. (2020). Long noncoding RNA HUPCOS promotes follicular fluid androgen excess in PCOS patients via aromatase inhibition. J. Clin. Endocrinol. Metab. *105*, dgaa060.
19. Li, D., Wang, X., Li, G., Dang, Y., Zhao, S., and Qin, Y. (2021). LncRNA ZNF674-AS1 regulates granulosa cell glycolysis and proliferation by interacting with ALDOA. Cell Death Discov. *7*, 107.
20. Kent, W.J., Sugnet, C.W., Furey, T.S., Roskin, K.M., Pringle, T.H., Zahler, A.M., and Haussler, D. (2002). The human genome browser at UCSC. Genome Res. *12*, 996–1006.
21. Kang, Y.J., Yang, D.C., Kong, L., Hou, M., Meng, Y.Q., Wei, L., and Gao, G. (2017). CPC2: a fast and accurate coding potential calculator based on sequence intrinsic features. Nucleic Acids Res. *45*, W12–W16.
22. Wang, L., Park, H.J., Dasari, S., Wang, S., Kocher, J.P., and Li, W. (2013). CPAT: coding-Potential Assessment Tool using an alignment-free logistic regression model. Nucleic Acids Res. *41*, e74.
23. Consortium, G.T. (2013). The genotype-tissue expression (GTEx) project. Nat. Genet. *45*, 580–585.
24. Zhang, Y., Yan, Z., Qin, Q., Nisenblat, V., Chang, H.M., Yu, Y., Wang, T., Lu, C., Yang, M., Yang, S., et al. (2018). Transcriptome landscape of human folliculogenesis reveals oocyte and granulosa cell interactions. Mol. Cell *72*, 1021–1034 e1024.
25. Mercer, T.R., Dinger, M.E., and Mattick, J.S. (2009). Long non-coding RNAs: insights into functions. Nat. Rev. Genet. *10*, 155–159.
26. Li, J.H., Liu, S., Zhou, H., Qu, L.H., and Yang, J.H. (2014). starBase v2.0: decoding miRNA-ceRNA, miRNA-ncRNA and protein-RNA interaction networks from large-scale CLIP-Seq data. Nucleic Acids Res. *42*, D92–D97.
27. El-Hayek, S., and Clarke, H.J. (2016). Control of oocyte growth and development by intercellular communication within the follicular niche. Results Probl. Cell Differ. *58*, 191–224.
28. Bansal, H., Bansal, S., Rao, M., Foley, K.P., Sang, J., Proia, D.A., Blackman, R.K., Ying, W., Barsoum, J., Baer, M.R., et al. (2010). Heat shock protein 90 regulates the expression of Wilms tumor 1 protein in myeloid leukemias. Blood *116*, 4591–4599.
29. Schopf, F.H., Biebl, M.M., and Buchner, J. (2017). The HSP90 chaperone machinery. Nat. Rev. Mol. Cell Biol. *18*, 345–360.
30. Wu, G., Yang, Z., Chen, Y., Li, X., Yang, J., and Yin, T. (2020). Downregulation of Lnc-OC1 attenuates the pathogenesis of polycystic ovary syndrome. Mol. Cell. Endocrinol. *506*, 110760.
31. Hu, W.L., Jin, L., Xu, A., Wang, Y.F., Thorne, R.F., Zhang, X.D., and Wu, M. (2018). GUARDIN is a p53-responsive long non-coding RNA that is essential for genomic stability. Nat. Cell Biol. *20*, 492–502.
32. Sang, B., Zhang, Y.Y., Guo, S.T., Kong, L.F., Cheng, Q., Liu, G.Z., Thorne, R.F., Zhang, X.D., Jin, L., and Wu, M. (2018). Dual functions for OVAAL in initiation of RAF/MEK/ERK prosurvival signals and evasion of p27-mediated cellular senescence. Proc. Natl. Acad. Sci. U S A *115*, E11661–E11670.
33. Zhang, D., Zhang, X., Zeng, M., Yuan, J., Liu, M., Yin, Y., Wu, X., Keefe, D.L., and Liu, L. (2015). Increased DNA damage and repair deficiency in granulosa cells are associated with ovarian aging in rhesus monkey. J. Assist. Reprod. Genet. *32*, 1069–1078.
34. Titus, S., Li, F., Stobezki, R., Akula, K., Unsal, E., Jeong, K., Dickler, M., Robson, M., Moy, F., Goswami, S., et al. (2013). Impairment of BRCA1-related DNA double-strand break repair leads to ovarian aging in mice and humans. Sci. Transl. Med. *5*, 172ra121.
35. Dou, X., Guo, T., Li, G., Zhou, L., Qin, Y., and Chen, Z.J. (2016). Minichromosome maintenance complex component 8 mutations cause primary ovarian insufficiency. Fertil. Steril. *106*, 1485–1489 e1482.
36. Guo, T., Zhao, S., Zhao, S., Chen, M., Li, G., Jiao, X., Wang, Z., Zhao, Y., Qin, Y., Gao, F., et al. (2017). Mutations in MSH5 in primary ovarian insufficiency. Hum. Mol. Genet. *26*, 1452–1457.
37. Weinberg-Shukron, A., Rachmiel, M., Renbaum, P., Gulsuner, S., Walsh, T., Lobel, O., Dreifuss, A., Ben-Moshe, A., Zeligson, S., Segel, R., et al. (2018). Essential role of BRCA2 in ovarian development and function. N. Engl. J. Med. *379*, 1042–1049.
38. Qin, Y., Zhang, F., and Chen, Z.J. (2019). BRCA2 in ovarian development and function. N. Engl. J. Med. *380*, 1086.
39. Wang, X., Zhang, X., Dang, Y., Li, D., Lu, G., Chan, W.Y., Leung, P.C.K., Zhao, S., Qin, Y., and Chen, Z.J. (2020). Long noncoding RNA HCP5 participates in premature ovarian insufficiency by transcriptionally regulating MSH5 and DNA damage repair via YB1. Nucleic Acids Res. *48*, 4480–4491.
40. Li, X., and Heyer, W.D. (2008). Homologous recombination in DNA repair and DNA damage tolerance. Cell Res. *18*, 99–113.
41. West, S.C. (2003). Molecular views of recombination proteins and their control. Nat. Rev. Mol. Cell Biol. *4*, 435–445.
42. Ma, J.Y., Feng, X., Tian, X.Y., Chen, L.N., Fan, X.Y., Guo, L., Li, S., Yin, S., Luo, S.M., and Ou, X.H. (2019). The repair of endo/exogenous DNA double-strand breaks and its effects on meiotic chromosome segregation in oocytes. Hum. Mol. Genet. *28*, 3422–3430.
43. Stringer, J.M., Winship, A., Zerafa, N., Wakefield, M., and Hutt, K. (2020). Oocytes can efficiently repair DNA double-strand breaks to restore genetic integrity and protect offspring health. Proc. Natl. Acad. Sci. U S A *117*, 11513–11522.
44. Luo, W., Guo, T., Li, G., Liu, R., Zhao, S., Song, M., Zhang, L., Wang, S., Chen, Z.J., and Qin, Y. (2020). Variants in homologous recombination genes EXO1 and RAD51 related with premature ovarian insufficiency. J. Clin. Endocrinol. Metab. *105*, dgaa505.
45. Gao, F., Zhang, J., Wang, X., Yang, J., Chen, D., Huff, V., and Liu, Y.X. (2014). Wt1 functions in ovarian follicle development by regulating granulosa cell differentiation. Hum. Mol. Genet. *23*, 333–341.
46. Chen, M., Zhang, L., Cui, X., Lin, X., Li, Y., Wang, Y., Wang, Y., Qin, Y., Chen, D., Han, C., et al. (2017). Wt1 directs the lineage specification of sertoli and granulosa cells by repressing Sf1 expression. Development *144*, 44–53.
47. Tang, J., Yan, T., Bao, Y., Shen, C., Yu, C., Zhu, X., Tian, X., Guo, F., Liang, Q., Liu, Q., et al. (2019). LncRNA GLCC1 promotes colorectal carcinogenesis and glucose metabolism by stabilizing c-Myc. Nat. Commun. *10*, 3499.
48. Guo, H., Zhao, L., Shi, B., Bao, J., Zheng, D., Zhou, B., and Shi, J. (2018). GALNT5 uaRNA promotes gastric cancer progression through its interaction with HSP90. Oncogene *37*, 4505–4517.
49. Mortimer, S.A., Kidwell, M.A., and Doudna, J.A. (2014). Insights into RNA structure and function from genome-wide studies. Nat. Rev. Genet. *15*, 469–479.

50. Bevilacqua, P.C., Ritchey, L.E., Su, Z., and Assmann, S.M. (2016). Genome-Wide analysis of RNA secondary structure. Annu. Rev. Genet. *50*, 235–266.

51. Somarowthu, S., Legiewicz, M., Chillon, I., Marcia, M., Liu, F., and Pyle, A.M. (2015). HOTAIR forms an intricate and modular secondary structure. Mol. Cell *58*, 353–361.

52. Tsai, M.C., Manor, O., Wan, Y., Mosammaparast, N., Wang, J.K., Lan, F., Shi, Y., Segal, E., and Chang, H.Y. (2010). Long noncoding RNA as modular scaffold of histone modification complexes. Science *329*, 689–693.

53. Nishi, Y., Yanase, T., Mu, Y., Oba, K., Ichino, I., Saito, M., Nomura, M., Mukasa, C., Okabe, T., Goto, K., et al. (2001). Establishment and characterization of a steroidogenic human granulosa-like tumor cell line, KGN, that expresses functional follicle-stimulating hormone receptor. Endocrinology *142*, 437–445.

54. Yan, H., Zhang, J., Wen, J., Wang, Y., Niu, W., Teng, Z., Zhao, T., Dai, Y., Zhang, Y., Wang, C., et al. (2018). CDC42 controls the activation of primordial follicles by regulating PI3K signaling in mouse oocytes. BMC Biol. *16*, 73.

OMTN, Volume *26*

Supplemental information

lncRNA *DDGC* participates in premature ovarian insufficiency through regulating *RAD51* and *WT1*

Duan Li, Weiwei Xu, Xiaoyan Wang, Yujie Dang, Lan Xu, Gang Lu, Wai-Yee Chan, Peter C.K. Leung, Shidou Zhao, and Yingying Qin

Supplementary Figure 1

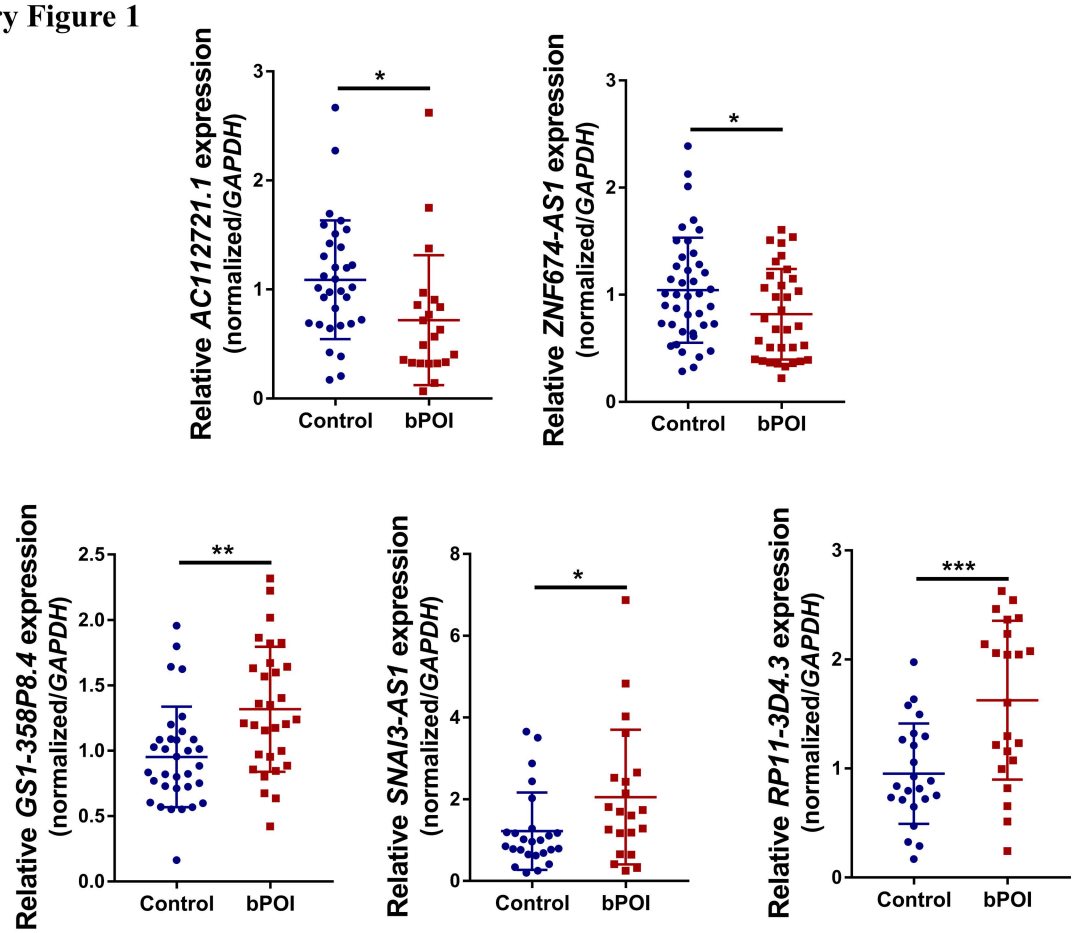

Supplementary Figure 1. The expression levels of lncRNAs were validated by qRT-PCR in GCs from controls and bPOI patients. Ct values were normalized to *GAPDH*. Data are presented as the mean ± SD. *P < 0.05, **P < 0.01, ***P < 0.001 by two-tailed Student's t-test.

Supplementary Figure 2

A

CPC2

ID	Label	Coding probability	Peptide length(aa)	Fickett score	Isoelectric point	ORF integrity	Details
ENST00000464929.5	noncoding	0.051056	73	0.32494	11.4901733398	complete	View

CPAT

Result for species name : hg19 with job ID :1590583809

Data ID	Sequence Name	RNA Size	ORF Size	Ficket Score	Hexamer Score	Coding Probability	Coding Label
0	ENST00000464929.5	819	219	0.5972	-0.0726352545543	0.012345255995295	no

B

Maximum (TPM)	Average (TPM)	Median (TPM)	CV	τ-Value	Expression Breadth
1.403	0.368	0.335	0.893	0.752	53

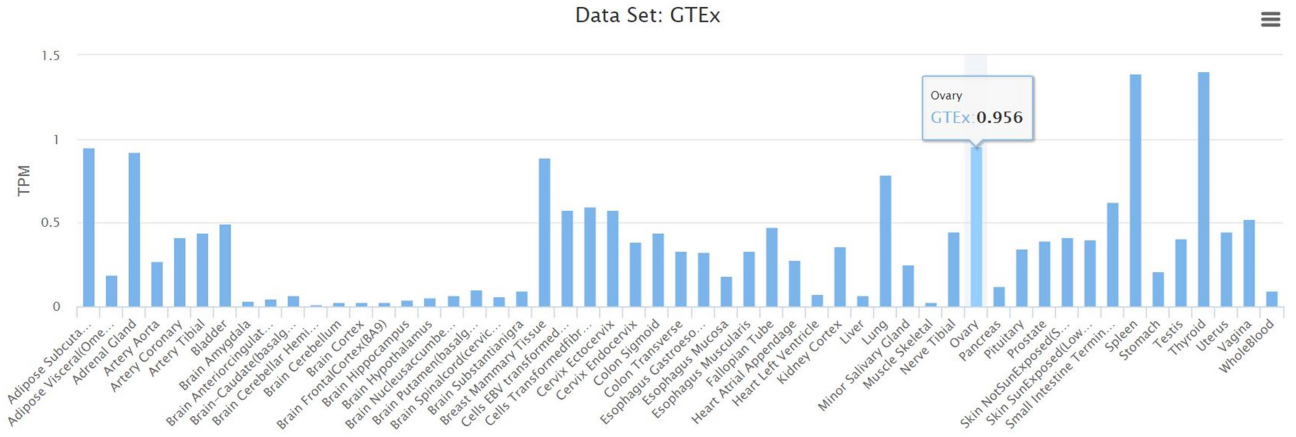

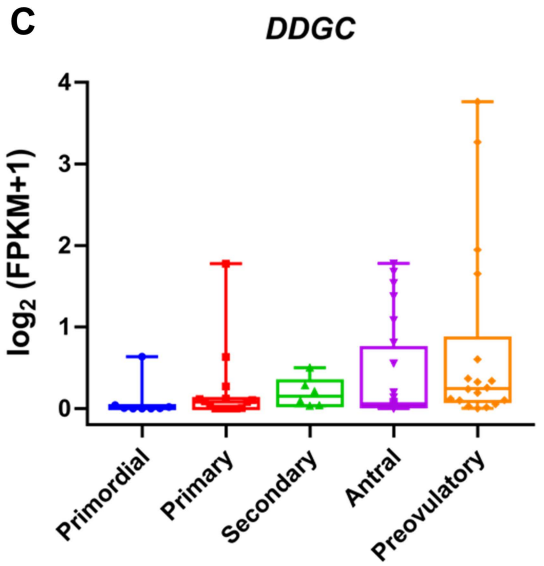

Supplementary Figure 2. (A) The coding probability of *DDGC* was assessed by the Coding Potential Calculator (CPC2) and Coding-Potential Assessment Tool (CPAT). **(B)** The expression levels of *DDGC* in multiple human tissues. Data are based on Genotype-Tissue Expression (GTEx) resources. **(C)** The expression of DDGC in human granulosa cells during folliculogenesis.

Supplementary Figure 3

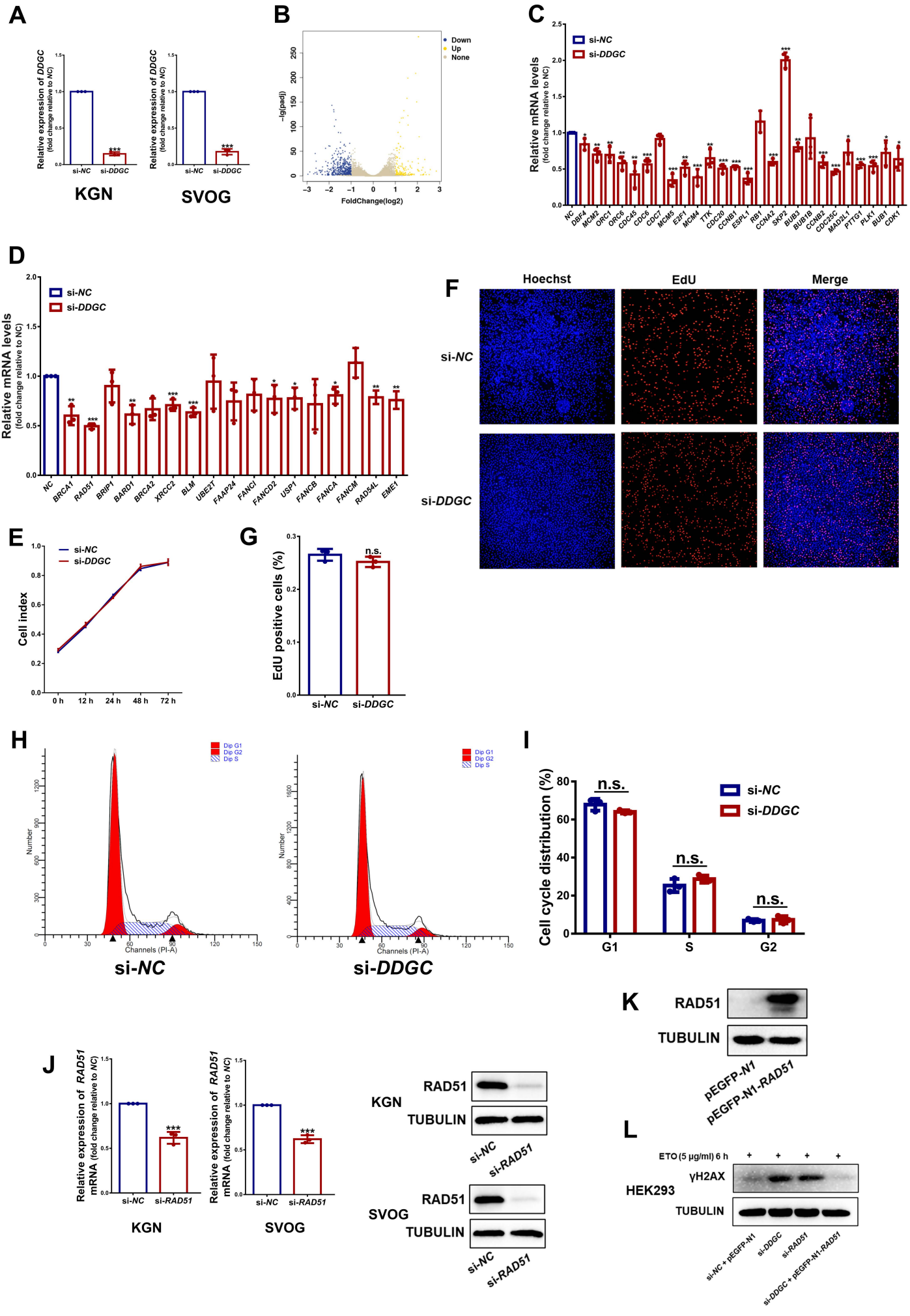

Supplementary Figure 3. (A) The efficiency of *DDGC* silencing in KGN and SVOG cells was measured by qRT-PCR. **(B)** Volcano plot of differentially expressed mRNAs between *DDGC*-silenced (n = 2) and negative control KGN cells (n = 2). **(C, D)** qRT-PCR was used to validate the expression level of genes involved in cell cycle progression and DNA damage repair in DDGC-silenced and negative control KGN cells. **(E)** Cell viability of *DDGC*-silenced and negative control KGN cells was determined with the CCK8 assay. The results are expressed as the mean ± SD (n = 3). **(F, G)** The proliferative ability of *DDGC*-silenced and negative control KGN cells was measured using an EdU staining assay. The results are expressed as the mean ± SD (n = 3). n.s. = not significant by two-tailed Student's t-test. **(H, I)** The cell cycle distribution of *DDGC*-silenced and negative control KGN cells was determined by flow cytometry analysis. The results are expressed as the mean ± SD (n = 3). Two-tailed Student's t-test. **(J)** *RAD51* mRNA and protein levels in *RAD51*-silenced and negative control KGN and SVOG cells were measured by qRT-PCR and western blot, respectively. **(K)** The RAD51 protein levels in *pEGFP-N1-RAD51* and *pEGFP-N1*-transfected HEK293 cells were measured by western blot. **(L)** The expression of γH2AX in *DDGC*-silenced, *RAD51*-silenced, co-transfected, and negative control HEK293 cells was measured by western blot. All qRT-PCR values were obtained from triplicate experiments and expressed as the mean ± SD (n = 3). *P < 0.05, **P < 0.01, ***P < 0.001, n.s. = no significance by two-tailed Student's t-test.

Supplementary Figure 4

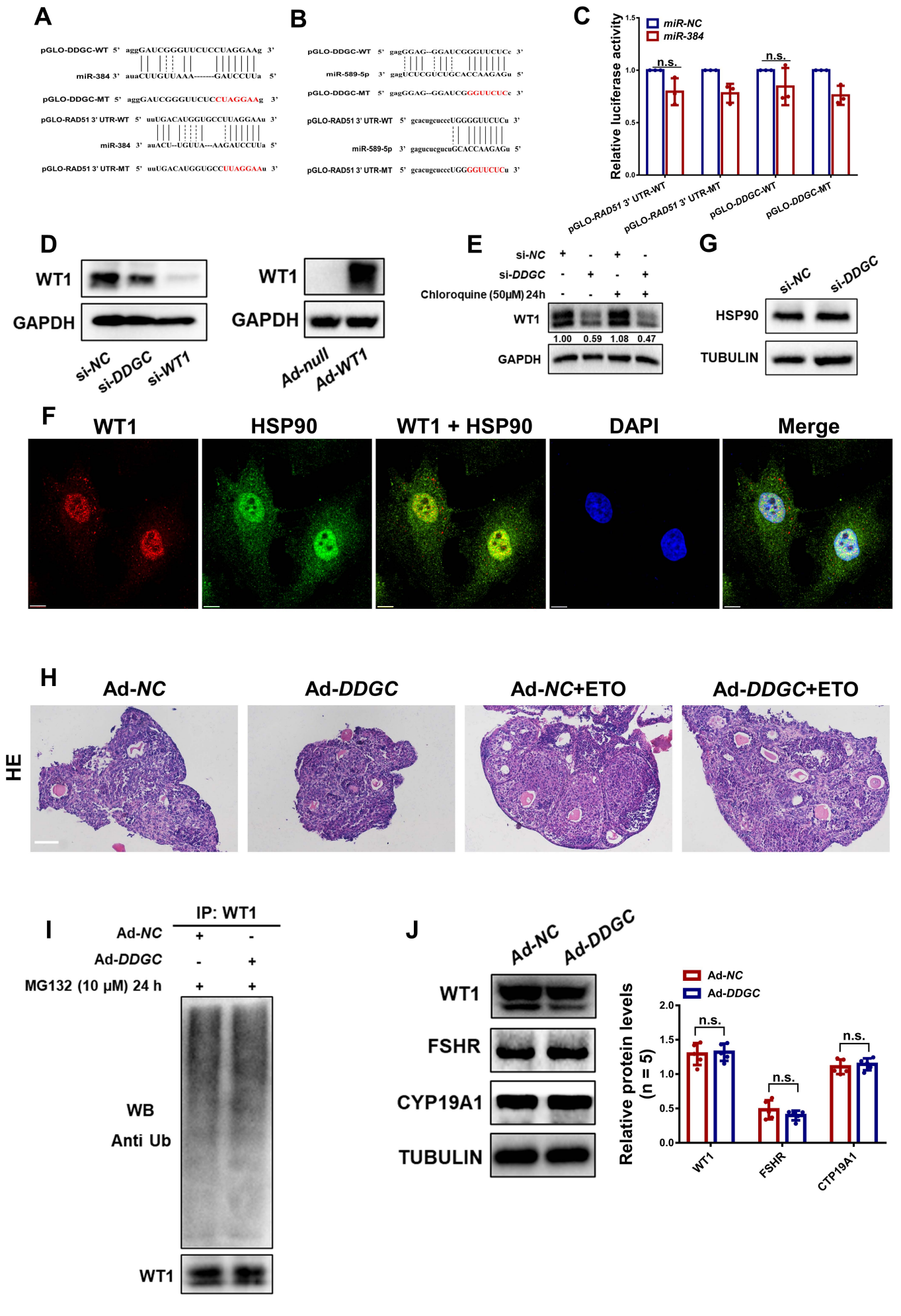

Supplementary Figure 4. (A, B) Luciferase reporter vectors were constructed by cloning the wild-type *DDGC* and *RAD51* mRNA 3' UTR sequences or MT sequences into the pmirGLO plasmid. The red nucleotides represent deleted sequences of the target sites. **(C)** Luciferase activity was analyzed at 48 h after co-transfection of reporter vectors and *miR-384* or negative control into HEK293 cells. Results are expressed as the mean ± SD (n = 3). n.s. = no significance by two-tailed Student's t-test. **(D)** The protein levels of WT1 in *DDGC*-silenced, *WT1* silenced, *WT1*-overexpressing, and negative control KGN cells were measured by western blot. **(E)** The protein levels of WT1 in *DDGC*-silenced and negative control KGN cells was measured by western blot at 24 h after the addition of chloroquine. **(F)** Subcellular localization of WT1 and HSP90 protein was confirmed by immunofluorescence assay. Scale bars = 10 μm. **(G)** The protein levels of HSP90 in *DDGC*-silenced and negative control KGN cells were measured by western blot. **(H)** Representative histological sections of *in vitro* cultured ovaries after *DDGC* over-expression. Scale bar = 50 μm. **(I)** Western blot showing the polyubiquitination level of WT1 in DDGC-overexpressed and negative control in vitro cultured ovaries at 24 h after the addition of MG132. **(J)** The protein levels of WT1, FSHR and CYP19A1 in *DDGC*-overexpressed and negative control mice ovaries were measured by western blot. Relative protein levels are expressed as the mean ± SD (n = 5). n.s. = no significance by two-tailed Student's t-test.

Supplementary Table 1. Fold change of lncRNAs validation

Gene (homo sapiens)	Fold change	P value
AC112721.1	1.59	0.024
ZNF674-AS1	1.27	0.041
DDGC	2.12	0.007
GS1-358P8.4	1.34	0.001
SNAI3-AS1	1.77	0.038
RP11-3D4.3	1.46	<0.001

Supplementary Table 2. List of primers used in this study

Gene (homo sapiens)	Forward (5'-3')	Reverse (5'-3')
AC112721.1	ACAGCAGCCCTAGCAAACTAAC	CCTGAGGAACGTGTAAACTGG
ZNF674-AS1	CCATGCCAGCATTTGCTATTCA	GGGCTTGAGGCTCTAAAGATGT
DDGC	CAGAGCATGGTCATTCAACATT	TCTAGGGAAACCATCTTGGAGA
GS1-358P8.4	TCATTGAATAGTGTGGGCTGCT	CCTTTCCTCCACCTCTGAAACA
SNAI3-AS1	CATCGCTCCCTCTACACGAG	TCCTTCTTGAGGGGTTGAGTTA
RP11-3D4.3	AGGATCAGAGCTTTGCCTTCAA	TATCACCAACTTGGGTGGTCTC
GAPDH	GGAGCGAGATCCCTCCAAAAT	GGCTGTTGTCATACTTCTCATGG
DBF4	GGGCAAAAGAGTTGGTAGTGG	ACTTATCGCCATCTGTTTGGATT
MCM2	ATGATCGAGAGCATCGAGAACC	GCCAAGTCCTCATAGTTCACCA
ORC1	ACCGAGATTCACATCCAGATTGG	CGAGCACGTTTCTTAGGAGGA
ORC6	ACAAGGAGACATATCAGAGCTGT	AGTGGCCTGGATAAGTCAAGAT
CDC45	GTGGGCCATCGTTGGACTAAC	TCAAAGGAGATCCGTGTGCAG
CDC6	ACCTATGCAACACTCCCCATT	TGGCTAGTTCTCTTTTGCTAGGA
CDC7	GAGGCGTCTTTGGGGATTCAG	GGTCCTACTTGTAACTGTGCTG
MCM5	ATGTCGGGATTCGACGATCCT	CCAGGTTGTAATGCCGCTTG
E2F1	CGTGGACTCTTCGGAGAACTTT	TGATGGTGGTGGTGACACTATG
MCM4	TGAACCTCTATACATGCAACGAC	CAGGGTAACGGTCAAAGAAGATT
TTK	CGCAGCTTTCTGTAGAAATGGA	GCAACAAACTCAACCAGTCCTC
CDC20	GCACAGTTCGCGTTCGAGA	CTGGATTTGCCAGGAGTTCGG
CCNB1	TTGGGGACATTGGTAACAAAGTC	ATAGGCTCAGGCGAAAGTTTTT
ESPL1	CTTGAAGGAGTTCCTGTCCAACC	TGGGGTAGACACTAAGTAGCCA
RB1	CTCTCGTCAGGCTTGAGTTTG	GACATCTCATCTAGGTCAACTGC
CCNA2	GGATGGTAGTTTTGAGTCACCAC	CACGAGGATAGCTCTCATACTGT
SKP2	GCAAGACTTCTGAACTGCTGTC	TCCCATGAAACACCTGGAAAGT
BUB3	TACATTTGCCACAGGTGGTTCT	TCAAGTACATGGTGACTTGGGT

BUB1B	AAATGACCCTCTGGATGTTTGG	GCATAAACGCCCTAATTTAAGCC
CCNB2	TTGGCTGGTACAAGTCCACTC	TGGGAACTGGTATAAGCATTGTC
CDC25C	AAGTGGCCTATATCGCTCCC	CCCTGGTTAGAATCTTCCTCCA
MAD2L1	GGACTCACCTTGCTTGTAACTAC	GATCACTGAACGGATTTCATCCT
PTTG1	CTGTTCCGCTGTTTAGCTCTTG	TTTGATTGAAGGTCCAGACCCC
PLK1	AAAGAGATCCCGGAGGTCCTA	GGCTGCGGTGAATGGATATTTC
BUB1	TCCTTCAGATGCTTGAAGCCC	GAGGTCACTGTTGTACTCAGCA
CDK1	AAACTACAGGTCAAGTGGTAGCC	TCCTGCATAAGCACATCCTGA
BRCA1	TTGTTACAAATCACCCCTCAAGG	CCCTGATACTTTTCTGGATGCC
RAD51	CAACCCATTTCACGGTTAGAGC	TTCTTTGGCGCATAGGCAACA
RAD54L	TTGAGTCAGCTAACCAATCAACC	GGAGGCTCATACAGAACCAAGG
BRIP1	CTTACCCGTCACAGCTTGCTA	CACTAAGAGATTGTTGCCATGCT
BARD1	TCGCGTTGTACTAACATTCTGA	GACAGCTCATTGTCATGTAGCA
BRCA2	ACAAGCAACCCAAGTGTCAAT	TGAAGCTACCTCCAAAACTGTG
XRCC2	TCACCTGTGCATGGTGATATTCT	AGCTTTGGGATAGTCTGTGCTC
BLM	CAGACTCCGAAGGAAGTTGTATG	TTTGGGGTGGTGTAACAAATGAT
UBE2T	ATCCCTCAACATCGCAACTGT	CAGCCTCTGGTAGATTATCAAGC
FAAP24	GGCCACCAGTAACATGATCTCT	AAAGTCTGGTGTCAAGCCATCC
FANCI	CCACCTTTGGTCTATCAGCTTC	CAACATCCAATAGCTCGTCACC
FANCD2	AAAACGGGAGAGAGTCAGAATCA	ACGCTCACAAGACAAAAGGCA
USP1	ATGCCTGGTGTCATACCTAGT	CAGTCCCACAAATGGTAACAAGT
FANCB	ATGAAGGATGGCCTAAGGGTC	ACACACTAACAACTTTGCCAGT
FANCA	TTTGCTTGAGGTAGAAGGTCCA	CCCGGCTGAGAGAATACCCA
FANCM	TCGTGACGGTGGTTACAACAC	ACAAGACGAATTGGGCTCTTC
MALAT1	AAAGTCCGCCATTTTGCCAC	CTCACAAAACCCCCGGAACT
LMNB1	GAAAAAGACAACTCTCGTCGCA	GTAAGCACTGATTTCCATGTCCA
β-actin	ACAGAGCCTCGCCTTTGCC	GAGGATGCCTCTCTTGCTCTG
FSHR	AAAGCTGCCTACTCTGGAAAAG	GACCCCTAGCCTGAGTCATATAA
CYP19A1	TGGAAATGCTGAACCCGATAC	AATTCCCATGCAGTAGCCAGG
WT1	CACAGCACAGGGTACGAGAG	CAAGAGTCGGGGCTACTCCA
Gene (Mus musculus)	**Forward (5'-3')**	**Reverse (5'-3')**
Rad51	AAGTTTTGGTCCACAGCCTATTT	CGGTGCATAAGCAACAGCC
Gapdh	AGGTCGGTGTGAACGGATTTG	TGTAGACCATGTAGTTGAGGTCA
Primers for in vitro transcription		
DDGC AS	CTAGCTAGCATTTAAAATAGAAATTTA	ATTTGCGGCCGCGCCACACACCCCGAGCCC

Supplementary Table 3. Oligonucleotides sequences used in this study

siRNAs	Sense(5'-3')
si-*NC*	UUCUCCGAACGUGUCACGUTT
si-*DDGC*	GGAGAGAAACAGGUAGCAATT
si-*RAD51*	CCAACGAUGUGAAGAAAUUTT
si-*WT1*	GCUUACCCAGGCUGCAAUATT
Biotin labelled miRNAs or probes	
Bio-NC	UUCUCCGAACGUGUCACGUTT
Bio-589-5p	UGAGAACCACGUCUGCUCUGAG
Biotin-DDGC-1	CAUACAUCUGUCAUGUAACACU
Biotin-DDGC-2	CAUACUGAAACUUCCUAGGAGA
Biotin-DDGC-3	AGGUAGUAGCUUCUAGGGAAAC
Biotin-DDGC-4	UGCUACCUGUUUCUCUCCUCAAUCA
Biotin-DDGC-5	UUGUAUAUCUGGUUUCUAAGAAUGC
Biotin-NC-probe	GUGUAACACGUCUAUACGCCCA

Supplementary Table 4. List of antibodies used in this study

Antibody	Supplier	Catalog#	Application
Phospho-Histone H2A.X (Ser139)	Cell Signaling Technology	9718S	WB/IF
GAPDH	Proteintech	60004-1-Ig	WB
PARP (Cleaved Asp214, Asp215)	Invitrogen	44-698G	WB
α-Tubulin	Proteintech	66031-1-Ig	WB
BRCA2	Abcam	ab27976	WB
BARD1	Santa Cruz	sc-74559	WB
BRCA1	Cell Signaling Technology	#9010	WB
Rad51 (D4B10) Rabbit mAb	Cell Signaling Technology	8875S	WB
β-Actin	Proteintech	66009-1-Ig	WB
Anti-Argonaute-2 antibody [EPR10411]	Abcam	ab186733	RIP
FSHR	Proteintech	22665-1-AP	WB
Aromatase (D5Q2Y) Rabbit mAb	Cell Signaling Technology	#14528	WB
FoxO1 (C29H4) Rabbit mAb	Cell Signaling Technology	2880T	WB
Anti-Wilms Tumor Protein antibody	Abcam	ab89901	WB/IF
WT1 (F-6)	Santa Cruz	sc-7385	IP
Ubiquitin (P4D1) Mouse mAb	Cell Signaling Technology	3936T	WB
HSP90	Abcam	ab13492	IP/RIP
HSP90 (C45G5) Rabbit mAb	Cell Signaling Technology	#4877	WB/IF
Anti-Lamin B1 antibody	Abcam	ab16048	WB
Anti-Aromatase	Abcam	ab18995	WB